MŰEGYETEM 1782

MASTER THESIS

Spin Diffusion and Transmission Electron Spin Resonance in Lithium

Bence Bernáth

Supervisor: Ferenc Simon
Professor
BME Department of Physics

Budapest University of Technology and Economics

2015.

Contents

A szakdolgozat kiírása

A spintronika az elektronika leváltását ambícionáló terület, mely az elektron spinjét használná mint információ hordozó egység. A területen számos alapkutatásbeli kérdés áll megválaszolásra illetve számos új anyag spintronikai felhasználási potenciálját kell és lehet megvizsgálnunk. A módszerek között igen fontos a mágneses rezonancia, melynek segítségével a spin-relaxációs idők közvetlenül meghatározhatóak. A vizsgálatokhoz elengedhetetlen a meglévő berendezések paramétereinek javítása ill. a kísérleti tartományaik kiterjesztése. A jelentkező érdeklődésének is megfelelően választhat az alábbi résztémák közül akár többet is: - nagyfrekvenciás (18-35 GHz) elektron spin rezonancia (ESR) spektrométer kifejlesztése - nagyfrekvenciás optikailag detektált mágneses rezonancia spektrométer fejlesztése - 9 GHz-es ESR berendezés működésének kiterjesztése 2 K-ig. - az ún. transzmissziós ESR berendezés kifejlesztése a vékony filmeken történő spin-transzport mérésekhez - egyéb alternatív, pl. rezisztíven detektált ESR mérések megtervezése és elvégzése.

Önállósági nyilatkozat

Alulírott Bernáth Bence, a Budapesti Műszaki és Gazdaságtudományi Egyetem hallgatója kijelentem, hogy ezt a szakdolgozatot meg nem engedett segédeszközök nélkül, saját magam készítettem, és csak a megadott forrásokat használtam fel. Minden olyan szövegrészt, adatot, diagramot, ábrát, amelyet azonos értelemben más forrásból átvettem, egyértelműen, a forrás megadásával megjelöltem.

Budapest, 2015. május 22.

Bernáth Bence

Köszönetnyilvánítás

Hálás vagyok témavezetőmnek, Simon Ferencnek, aki példamutató türelmével és lelkesedésével tanított és segített a munkámban. A munkához és a tudományhoz való hozzáállása mindig ösztönzőleg hatott rám.
Köszönöm Jánossy Andrásnak iránymutatásait és észrevételeit a TESR spektrométer fejlesztésével kapcsolatban
Köszönöm Bacsa Sándornak, Horváth Bélának és Kovács Tamásnak a mikrohullámú üreg elkészítésében nyújtott segítségét.
Külön köszönöm Márkus Bencének a LaTeX-ban nyújtott segítségét és azt, hogy megtanított a dry-box használatára. Gyüre Balázsnak köszönöm, hogy bevezetett a mikrohullámú technika világába és minden segítségét amelyet a kísereletek során nyújtott nekem. Köszönöm Szolnoki Lénárdnak és Dzsaber Száminak a szakmai eszmecseréket.
Köszönöm Váczi Viktornak, hogy segített a szimuláció megírásában.
Hálával tartozom családomnak és barátaimnak akik idáig minden döntésemben szabadon hagytak, illetve középiskolai matematika és fizika tanáraimnak Pintér Ambrusnak, Hirka Antalnak, akik megtanítottak arra, hogy a problémákat szeretnünk kell.
I acknowledge Prof. F. I. B. (Tito) Williams for enlightening discussions about microwave circuitry. His inspiration provided a major leap to understand the physics of microwave mixers and detectors.
Financial support by the European Research Council Grant Nr. ERC-259374-Sylo is acknowledged.

Chapter 1

Introduction and motivations

Information processing and storage using electron spins, commonly referred to as spintronics, is an actively studied field. Spintronics utilizes the prolonged conservation of the spin quantum number, as the spin-relaxation time (T_1) dominates over the momentum relaxation time (τ) by several orders of magnitude. Therefore determining spin-relaxation time and spin free-path in solid-states, both theoretical and experimental ways, is one of the most important aim of fundamental research on spintronics.

The recent discovery of graphene directed the attention of spintronics research toward carbon nanostructures. The weak spin-orbit coupling of carbon atoms and its large mobility make graphene a viable candidate for future spintronics applications, as demonstrated in nonlocal spin valve and Hanle spin precession experiments where spin relaxation time and spin diffusion time were measured by transport methods [30, 29]. Electron spin resonance spectroscopy is also able to measure spin relaxation time [5]. Because of its contactless nature the conventional spectrometer is not able to measure transport phenomena directly.

A compelling alternative and complementary method to the above list is the so-called transmission electron spin resonance (TESR) [7]. This method is based on the fact that conduction electrons diffuse in a metal and when they possess a non equilibrium magnetization, this can be carried over longer distances. In practice the experiment is realized by having two ESR cavities which share a common sidewall which is covered (or is partly covered) by the metal under study. TESR in fact combines the advantages of both spectroscopic (the contactless nature) and transport approaches (the fact that the diffusion length is directly obtained) which makes it a compelling and complementary tool in the spintronics characterization of metals and samples that have weak spin-orbit coupling thus electron diffusion is observable.

The motivation for the present work is two fold. First, we plan to carry our TESR experiments on novel nanonstructural materials, such as e.g. doped graphene. The present development constitutes the starting points for such activities. Second, much as the TESR method was developed in the 1960-

1970's a more modern approach is worth. Such as e.g. the use of low noise preamplifiers, lock-in amplifiers and IQ mixers, which allow the simultaneous detection of the quadrature microwave signals.

We herein present the construction of a TESR system and the first results on lithium. Lithium has a long spin relaxation time it is therefore ideal for the TESR experiments. We clearly identify the TESR signal after performing several critical control experiments. By quadrature detection we show that TESR satisfies the linear response theory.

Chapter 2

Theoretical and technical background

Electron Spin Resonance (ESR) Spectroscopy has become a wide-spread technique since its discovery in the 1940's by Y.K. Zavoisky [1]. In solid-state physics, it is generally utilized to investigate magnetic interactions and spin dynamics in matter. This technique gives us possibility to measure spin relaxation time, resonance frequency and spin-susceptibility. Our aim is to introduce a method measuring conduction electron spin transmission based on ESR technique. In order to understand transmission electron spin resonance (TESR), we need to know how magnetic resonance and transport phenomena emerge in conductive samples.

2.1 Electron Spin Resonance

Electron Spin Resonance Spectroscopy is an appropriate method to make contactless investigation on magnetic properties of matter, a free-radical of molecule or conduction electrons.

The effect of external magnetic field in Hamilton operator is

$$H_{\text{ext}} = -\boldsymbol{\mu}\mathbf{B} \tag{2.1}$$

where $\boldsymbol{\mu}$ is the complete magnetic moment of an atomic system. Let us take the simplest case, one free electron which has dimensionless spin $\mathbf{S}$ appearing in its magnetic moment.

$$\boldsymbol{\mu} = -g_e \mu_B \mathbf{S} \tag{2.2}$$

$\mu_B = 9.27 \cdot 10^{-24}\ \frac{\mathrm{J}}{\mathrm{T}}$ is the Bohr magneton, $g_e = 2.0023$ is the free electron g-factor, $\hbar$ is the Planck constant. Without magnetic field, two spin quantum states are degenerated with quantum numbers of $m_s = \pm\frac{1}{2}$. The external magnetic field $\mathbf{B}$ (often referred as $\mathbf{B}_0$) lifts degeneracy. Energy difference between the two states is $\Delta E = E_{+\frac{1}{2}} - E_{-\frac{1}{2}} = g_e \mu_B B_0$. The phenomenon of splitting energy levels in magnetic fields is the Zeeman effect. Here an important quantity emerged called free electron gyromagnetic ratio $\gamma_e = -g_e \frac{\mu_B}{\hbar} = g_e \frac{-e}{2m_e}$. The

e is the elementary charge of the electron, m_e is the mass of the electron. This ratio says how much energy is neccessary for a transition between the split states at a given magnetic field. $\frac{\gamma_e}{2\pi} \approx 28\ \frac{\mathrm{GHz}}{\mathrm{T}}$ means that we need 28 GHz frequency electromagnetic wave in 1 T to generate transition. In our case we use approximately 0.3 T and 9 GHz.

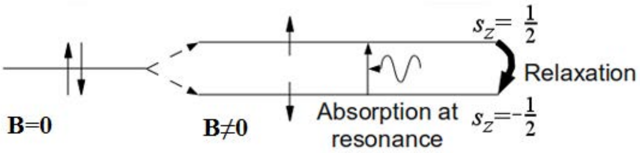

Figure 2.1: Zeeman splitting of an electron induced by an external magnetic field

In general, the energy splitting of the electron leads to the Zeeman Hamiltonian

$$H_{Zeeman} = -\boldsymbol{\mu}\mathbf{B}_0 = g_J\mu_B\mathbf{J}\mathbf{B}_0. \tag{2.3}$$

$\mathbf{J} = \mathbf{L} + \mathbf{S}$ is the total angular momentum, g_J is the Landé g-factor. Hence the energy difference between adjacent states $\Delta E = g_J\mu_B B_0$. For conduction electrons, the expectation value of orbital angular momentum $\mathbf{L}$ can be neglected. Having $\hbar\omega$ exciting energy, resonant absorption and transition happens

$$\Delta E = g_e\mu_B B_0 = \hbar\gamma_e B_0 = \hbar\omega. \tag{2.4}$$

Using Ehrenfest theorem for calculating time dependence of spin momentum

$$\frac{\mathrm{d}\langle\mathbf{S}\rangle}{\mathrm{d}t} = \frac{i}{\hbar}[H_{Zeeman}, \mathbf{S}] = \gamma_e\langle\mathbf{S}\rangle \times \mathbf{B}_0. \tag{2.5}$$

$\langle . \rangle$ indicates the quantum mechanical expectation value. The equation is similar to the classical case when $\mathbf{B}_0$ field causes torque on angular momentum. Therefore the magnetic moment precesses around the field with Larmor frequency $\omega_L = \gamma_e B_0$.

The resonant transition in ESR is caused by an alternating magnetic field from the microwave irradiation. We assume that $\mathbf{B}_0$ is parallel to $\mathbf{z}$ axis and the alternating field is a linearly polarized wave, $B_x = B_{x0}\cos(\omega t)$ along the $\mathbf{x}$ axis. Linearly polarized wave is the sum of two rotating components. Only one component $\mathbf{B}_1 = \frac{B_{x0}}{2}[\cos(\omega t)\mathbf{i} - \sin(\omega t)\mathbf{j}]$ which rotates consistent to the precession of the moment, induces absorption transition. In laboratory frame for the $\gamma\hbar\mathbf{J} = \boldsymbol{\mu}$ magnetic moment can be written as

$$\frac{\mathrm{d}\langle\boldsymbol{\mu}\rangle}{\mathrm{d}t} = \langle\boldsymbol{\mu}\rangle \times \gamma(\mathbf{B}_0 + \mathbf{B}_1) = \langle\boldsymbol{\mu}\rangle \times \gamma\mathbf{B}. \tag{2.6}$$

This equation does not yet explain the experimentally observed relaxation phenomena. The magnetic moment, due to the interactions, relaxes and stops precessing. It means that after a certain lapse of time, the magnetic moment and the magnetization $\mathbf{M} = \frac{\boldsymbol{\mu}}{V_{sample}}$ stands parallel to the external magnetic field and reaches its equilibrium value. The Bloch equations bring the best phenomenological description for this problem [2].

$$\frac{dM_z(t)}{dt} = \gamma[\mathbf{M} \times \mathbf{B}]_z + \frac{M_0 - M_z(t)}{T_1} \tag{2.7}$$

$$\frac{dM_x(t)}{dt} = \gamma[\mathbf{M} \times \mathbf{B}]_x - \frac{M_x(t)}{T_2} \tag{2.8}$$

$$\frac{dM_y(t)}{dt} = \gamma[\mathbf{M} \times \mathbf{B}]_y - \frac{M_y(t)}{T_2} \tag{2.9}$$

In general, T_1 (spin-lattice or longitudinal) and T_2 (spin decoherence or transversal) relaxation times do not have the same value, but in metals they are equal $T_1 = T_2$ [3]. By solving these equations in a frame of reference which rotates at an angular frequency ω, we have the x,y magnetization as

$$\begin{aligned} M'_x &= \frac{\chi_0\omega_0}{\mu_0} T_2 \frac{(\omega_0 - \omega)T_2}{1 + (\omega_0 - \omega)^2 T_2^2} B_1 \\ M'_y &= \frac{\chi_0\omega_0}{\mu_0} T_2 \frac{1}{1 + (\omega_0 - \omega)^2 T_2^2} B_1. \end{aligned} \tag{2.10}$$

Herein, the transition angular frequency is: $\omega_0 = \gamma_e B_0$. The rotating frame of reference is denoted as ’ and the equilibrium magnetization reads $M_0 = \frac{\chi_0 B_0}{\mu_0}$ where χ_0 is the static spin susceptibility, in metals it is the Pauli susceptibility which is temperature dependent.

$$\chi_0 = \chi_{\text{Pauli}} = \frac{1}{4}\mu_0 (g_e \mu_B)^2 \rho(\epsilon_F) \frac{1}{V_c} \tag{2.11}$$

where $\rho(\epsilon_F)$ is the density of states at Fermi energy and V_c is the unit cell volume. In the laboratory frame the magnetization reads:

$$M_x(t) = M'_x \cos(\omega t) + M'_y \sin(\omega t) \tag{2.12}$$

The proportional factors are the susceptibilities. Then the form of magnetization

$$M_x(t) = (\chi' \cos(\omega t) + \chi'' \sin(\omega t)) B_{x0} = \chi(\omega) B_x(t) \tag{2.13}$$

where $\chi(\omega)$ is dynamical susceptibility and

$$\chi = \chi' - \mathbf{i}\chi''. \tag{2.14}$$

The real part is the dispersive, while the imaginary part is the dissipative response. The absorption is proportional to χ'' . From the equations above the susceptibilities are the following

$$\chi' = \frac{1}{2}\chi_0\omega_0 T_2 \frac{(\omega_0 - \omega)T_2}{1 + (\omega_0 - \omega)^2 T_2^2} \tag{2.15}$$

$$\chi'' = \frac{1}{2}\chi_0\omega_0 T_2 \frac{1}{1+(\omega_0-\omega)^2 T_2^2}. \tag{2.16}$$

The dynamic susceptibilities are connected by Kramers-Kronig relations [14, 13]:

$$\chi'(\omega) = \frac{1}{\pi}P\int_{-\infty}^{\infty} \mathrm{d}\omega'\chi''(\omega')\frac{1}{\omega'-\omega} \tag{2.17}$$

$$\chi''(\omega) = -\frac{1}{\pi}P\int_{-\infty}^{\infty} \mathrm{d}\omega'\chi'(\omega')\frac{1}{\omega'-\omega} \tag{2.18}$$

where P denotes the Cauchy principal value. χ' is the Hilbert transform of $-\chi''$ [15, 16].

The ESR lineshape is a Lorentzian curve which is proportional to χ''. The calculations above are valid for non-metallic samples. For metallic samples the line shape is explained by the theory of Dyson called Conduction Electron Spin Resonance (CESR) [4].

After discussing the basics of the ESR theory, we discuss some technical aspects of the ESR signal detection. These are vital for the analysis of the experiments.

2.1.1 Power detected from ESR

It is a fact that an RLC circuit is a very good model of microwave cavity. If we put a sample in the cavity, the whole system can be an RLC system shown on 2.2.

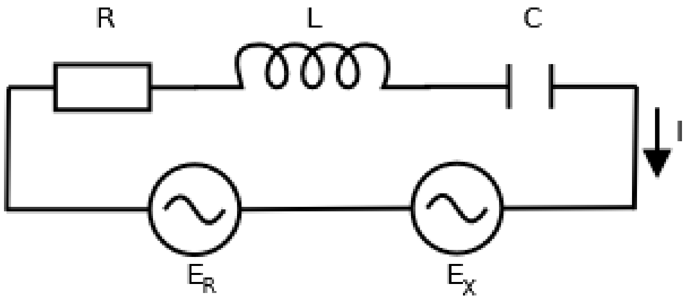

Figure 2.2: Equivalent circuit of an E.S.R. spectrometer cavity with sample having rotating magnetization.

L and C are assumed to resonate at the microwave frequency ω therefore their net impedance is zero. R expresses the losses within the cavity. We describe the ESR signal of a sample as an additional microwave source which generates microwaves inside the cavity. E_R and E_X define the two components of the so-called sample spin-generator voltage, E_R for the resistive or absorbing component proportional to χ'', E_X the reactive or dispersive component proportional to χ'. From now we follow the calculation of T.H. Wilmshurts

[8]. P_{a} is the available power from the two components

$$P_{\mathrm{a}} = \frac{E_{\mathrm{R}}^2}{8R} = \frac{E_{\mathrm{X}}^2}{8R}. \tag{2.19}$$

It is neccessary to express E_{R} and E_{X} in terms of P_{i} which is the power incident on the cavity. If the cavity is critically coupled this power fully dissipated in the cavity and no reflection is observed. Thus $P_{\mathrm{i}} = \frac{I^2R}{2}$. One can show that

$$E_{\mathrm{R}} = \frac{2\omega}{I}\int_{\mathrm{S}} \mathbf{M}'\mathbf{B}_1 dV \tag{2.20}$$

where the volume integral belongs to the sample. The available power from the spin generator is:

$$P_{\mathrm{a}} = \frac{(\omega\int_{\mathrm{S}} \mathbf{M}'\mathbf{B}_1 dV)^2}{2I^2R} \tag{2.21}$$

This equation is for the rotating frame of reference. For the laboratory frame

$$P_{\mathrm{a}} = \frac{\omega^2}{16}\left(\frac{\int_S \mathbf{M}\mathbf{B}_x dV}{P_{\mathrm{i}}}\right)^2 P_{\mathrm{i}} \tag{2.22}$$

holds. For resonance we obtain: $\mathbf{M} = \chi''\mathbf{B}_x/\mu_0$. The voltage developed by the sample at the detector is proportional[1] to $\sqrt{P_{\mathrm{a}}}$, so from now we express this term.

$$\sqrt{P_{\mathrm{a}}} = \frac{\omega\chi''\int_S \mathbf{B}_x^2 dV}{4P_{\mathrm{i}}\mu_0}\sqrt{P_{\mathrm{i}}} \tag{2.23}$$

The term $\frac{\omega\int_{\mathrm{S}} \mathbf{B}_x^2 dV}{P_i}$ is proportional to the product of cavity filling factor η and the Q-factor of the cavity. Definition of Q-factor of the cavity is

$$Q = \frac{\omega \cdot \text{Energy stored}}{\text{Power dissipated}}. \tag{2.24}$$

The energy stored in the magnetic field of the cavity is given by $\frac{\int_{\mathrm{C}} \mathbf{B}_x^2 dV}{2\mu_0}$ where the integral goes through the whole cavity. Thus $Q = \omega\frac{\int_{\mathrm{C}} \mathbf{B}_x^2 dV}{2\mu_0 P_{\mathrm{i}}}$ and

$$\sqrt{P_{\mathrm{a}}} = \frac{\chi''}{2}\cdot\frac{\int_{\mathrm{S}} \mathbf{B}_x^2 dV}{\int_{\mathrm{C}} \mathbf{B}_x^2 dV}\cdot Q\cdot\sqrt{P_{\mathrm{i}}} = \frac{\chi''}{2}\cdot\eta\cdot Q\cdot\sqrt{P_{\mathrm{i}}} = \frac{\chi''}{\sqrt{8}}\eta\sqrt{Q}\cdot\sqrt{\frac{\omega}{\mu_0}\int_C \mathbf{B}_x^2 dV} \tag{2.25}$$

where we define $\eta = \frac{\int_{\mathrm{S}} \mathbf{B}_x^2 dV}{\int_{\mathrm{C}} \mathbf{B}_x^2 dV}$ as cavity filling factor which indicates how efficiently the sample fills the available magnetic field in the cavity. When the sample is saturated by the microwave irradiation the equations above are no longer appropriate. Let $\mathbf{M}_{\mathrm{max}}$ denote the maximum microwave magnetization

---

[1] Commercial ESR spectrometers use mixer to detect microwaves. This method results microwave voltage, not the power.

obtainable without saturation. $\int_{\mathrm{S}} \mathbf{M} dV$ can be expressed as $\mathbf{M}_{\mathrm{max}} \int_{\mathrm{S}} h dV$, where h has the same spatial variation of $\mathbf{M}$ is dimensionless. Equation 2.22 then becomes

$$\sqrt{P_{\mathrm{a}}} = \frac{\omega}{4} \left(\int_{\mathrm{S}} \mathbf{B}_x^2 dV \frac{\int_{\mathrm{S}} h^2 dV}{P_i} \right)^{\frac{1}{2}} M_{max} \tag{2.26}$$

2.1.2 Mixer and quadrature detection

For sensitive detection the modern spectrometers use mixer technique to detect low signal with low noise level. Now we review the basics of mixers.

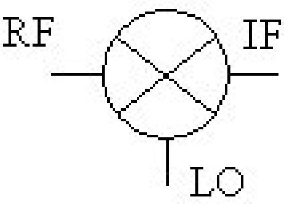

Figure 2.3: A general mixer

In a mixer three port meet: local oscillator (LO), radio frequency (RF) and intermediate frequency (IF). The term radio frequency generally refers the high frequency, in our case this is the signal with modulation coming from the cavity, so it is the order of 9 GHz. The LO has the same frequency as the source has. In our measurement the local oscillator is derived from the same source as the signal before the modulating process. The name of this method is homodyne detection. Although RF and LO are microwaves, we can handle them as alternatig voltages.

$$V_{\mathrm{LO}}(t) = A_{\mathrm{LO}} \cos(\omega_{\mathrm{LO}} t) \tag{2.27}$$

LO is neccessary part of the mixers and we can control its power.

$$V_{\mathrm{RF}}(t) = a(t) \cos(\omega_{\mathrm{RF}} t + \phi(t)) \tag{2.28}$$

Here $a(t)$ and $\phi(t)$ are time dependent parts and mean the amplitude and phase modulation. The output IF signal is proportional to the product of RF and LO signal in ideal case.

$$V_{\mathrm{IF}} = K A_{\mathrm{LO}} a(t) \cos(\omega_{\mathrm{LO}} t) \cos(\omega_{\mathrm{RF}} t + \phi(t)) \tag{2.29}$$

Where K is a conversion factor which expresses the loss. By trigonometric identities V_{IF} is written as

$$V_{\mathrm{IF}} = \frac{K A_{\mathrm{LO}}}{2} a(t) \cos[(\omega_{\mathrm{RF}} - \omega_{\mathrm{LO}})t + \phi(t)] + \frac{K A_{\mathrm{LO}}}{2} a(t) \cos[(\omega_{\mathrm{RF}} + \omega_{\mathrm{LO}})t + \phi(t)] \tag{2.30}$$

A tipical mixer contains low-pass filter therefore the high frequency part is neglectable.

$$V_{\mathrm{IF}} = \frac{KA_{\mathrm{LO}}}{2} a(t) \cos[(\omega_{\mathrm{RF}} - \omega_{\mathrm{LO}})t + \phi(t)] \tag{2.31}$$

As it is seen the IF signal has lower frequency and lower amplitude than RF but it contains all parameters for reconstructing the original signal. If we want IF signal with high amplitude we should enhance A_{LO}. However we must consider that the LO port can be saturated and from that point the IF signal will not be higher. The loss of downconversion is defined as

$$\frac{P_{\mathrm{IF}}}{P_{\mathrm{RF}}} = \left(\frac{KA_{\mathrm{LO}}}{2}\right)^2. \tag{2.32}$$

KA_{LO} has tipical value about 1. Loss in dB unit is about $10\log_{10}(\frac{1}{4}) = -6$dB. This value varies from -3dB ot -10dB. The quantity which indicates the loss of the mixer is conversion loss (CL):

$$CL = -10\log_{10}\left(\frac{P_{\mathrm{IF}}}{P_{\mathrm{RF}}}\right) \tag{2.33}$$

and its value varies from 3 dB to 10 dB. Obviously low CL is desirable. The formulas show that we must keep the LO power near the saturation power because if we work with less LO power the CL is increased [9].

In our measurement we use an IQ mixer (Marki IQ 0618) with which the quadrature detection is possible. The IQ mixer splits RF and LO in two equal part gives 90° shift for one of splitted LO. It has two output; "Q" indicates the quadrature signal that is product of shifted LO and RF, "I" output indicates the in-phase signal that is product if in-phase LO and RF. The resultant two components are perpendicular. Only with this type of detection we are able to measure Kramers-Kronig pairs of susceptibility simultaneously. In the master thesis we employ IQ mixer to justify the validity of the linear response theory. IQ mixer detection is also required when the LO and RF have different frequencies and the sign of the IF needs to be known, too. E.g. this is employed in pulsed ESR and NMR spectroscopies.

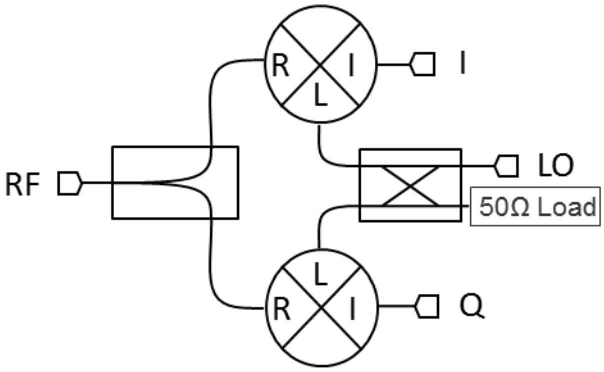

Figure 2.4: Schematics of an IQ mixer [10]

2.1.3 Relationship between the complex dynamic spin-susceptibility and microwave phase

As it was shown in the equations (2.10) and (2.13), the absorbative and dispersive susceptibilities are perpendicular. Thus voltages E_R and E_X are in phase quadrature. This situation is quite similar to an N.M.R. spectrometer circuit. The sample is in the coil and experiences the excitation provided by a coil which is driven by an ac current. The appropriate rotating component of the linearly polarized field sets up a rotating component of magnetization within the sample as (2.10) shows. This magnetization generates varying magnetic flux which induces an electromagnetic field in the coil. This excitation rotates the magnetization from along the z axis into the xy plane. The real part of the susceptibility χ' called in-phase component produces a voltage that leads the current. The imaginary part of the susceptibility χ'' called quadrature component gives a voltage in antiphase with the current. χ' introduces an effective inductance X into the coil and χ'' introduces a resistance(R) [8]. Therefore the signal of χ' and χ'' has 90° difference.

The detected signal always contains both dispersive and absorptive component, general detection systems[2] measure only one component according to the relative phase of source.

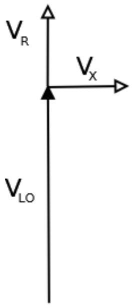

Figure 2.5: In-phase and quadrature phase relationships of local oscillator signal and and sample signal.

Thus we can select the absorptive or dispersive component by proper adjustement of the local oscillator phase. When we have detuned phase, the absorptive and dispersive components become mixed.

In Figure 2.6 the points A and B correspond to the width at half-height for the absorption signal. The f_0 indicates the resonance frequency. The vector diagram shows properly that far from the resonance frequency($f = 0$ or ∞) there is no dispersive and absorptive response at all.

In Figure 2.7 in (a) and (e) we observe the absorption signal with opposite sign and the dispersion signal is suppressed. In (b) and (d) the phase is shifted

---

[2] They are called mixers discussed in 2.1.2. They have a local oscillator (coming from the source) signal constantly and they receive the signal from the sample. It measures the product of the two signal that is why the phase difference between signals is very important.

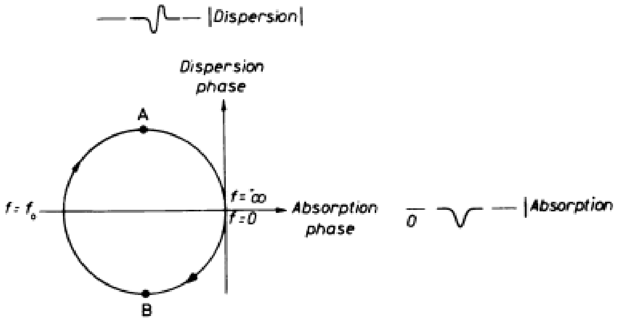

Figure 2.6: The relative phases of the dispersion and absorption signals, together with their variations of amplitude with frequency from Ref. [8].

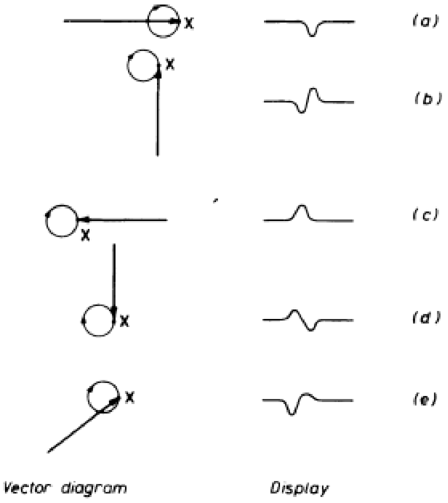

Figure 2.7: Effect of altering the phase of local oscillator signal from Ref.[8].

by ±90° to give observation of the dispersive and suppression of absorptive components. There is an intermediate phase (e) which mixes both absorption and dispersion.

2.2 Conduction Electron Spin Resonance

In the previous general discussion of ESR, the description assumed non-interacting spins, i.e. paramagnetic spins in an insulatig compound In metals the penetration of the electromagnetic field is limited because of the skin-effect and delocalized electrons. We have to take into account the diffusion of the electrons in and out of the skin depth to calculate resonance absorption and the special line shape. The experimental work of Kip and feher [5] and the theoretical description of Dyson [4] gives a proper explanation of these effects. We note that linear response theory is valid for CESR however diffusion makes the calculation difficult and there exists no compact lineshape for the general Dysonian curve.

From the Maxwell's equations we get a modified expression for the conductive medium:

$$\Delta\mathbf{B} = \mu\epsilon\frac{\partial^2\mathbf{B}}{\partial t^2} + \mu\sigma\frac{\partial\mathbf{B}}{\partial t}. \tag{2.34}$$

The solution of this equation can be a plane wave:

$$\mathbf{B}(x,t) = \mathbf{B}^0 e^{\mathrm{i}(kx-\omega t)} \tag{2.35}$$

where $\mathbf{B}^0$ is the amplitude of the ac magnetic field at the sample surface. After substituting, a complex wave number is given by

$$k = \sqrt{\mu\epsilon\omega^2 + \mathrm{i}\mu\sigma\omega} = \mathrm{i}\frac{1}{\delta_{\text{Skin}} + \kappa} \tag{2.36}$$

where $\kappa = \omega\left[\left(\frac{\epsilon\mu}{2}\right)\left(\sqrt{1+(\frac{\sigma}{\omega\epsilon})^2} - 1\right)\right]^{\frac{1}{2}}$. The general expression for the skin depth is $\delta_{\text{Skin}} = \frac{1}{\omega}\left[\left(\frac{\epsilon\mu}{2}\right)\left(\sqrt{1+(\frac{\sigma}{\omega\epsilon})^2} + 1\right)\right]^{-\frac{1}{2}}$ but for metals this expression can be simplified

$$\delta_{\text{Skin}} = \sqrt{\frac{2}{\mu\sigma\omega}} \tag{2.37}$$

where μ and ϵ are the total permeability and permittivity respectively and σ is the conductivity. If the electromagnetic waves propagates along the $\mathbf{x}$ axis, then the ac magnetic field strength is given by

$$\mathbf{B} \sim e^{-\frac{x}{\delta_{\text{Skin}}}} \cdot e^{\cdot\mathrm{i}(\kappa x-\omega t)} \tag{2.38}$$

in the sample. We emphasize that going through the $\mathbf{x}$ axis into the sample the phase of exciting electromagnetic field continuously changes, thus every plane perpendicular to the $\mathbf{x}$ axis gets different excitation. This fact results in a different line shape as compared to a non-metallic sample. According to Dyson, Kip and Feher we distinguish two main cases: region of normal and anomalous skin effect. This distinction is based on whether the mean free-path δ_{ℓ} is smaller (normal) or larger (anomalous) than the skin-depth. The latter occurs for very high frequency electromagnetic radiation (in the THz range) for very pure metals. The normal skin effect regime occurs in Li at room temperature and 9 GHz excitation so we focus on this regime only.

The general problems is to calculate the magnetization produced by a given $\mathbf{B}_1$, and to find a self-consistent solutions of Maxwell's equations to express the relationships between $\mathbf{B}_1$ and $\mathbf{M}$. The magnetization is carried around by the electrons as they diffuse in the metal. This fact makes the problem quite unusual and more involved. The assumptions of Dyson were the following:

1. All electrons which carry the magnetization lie at the top of the Fermi distribution of conduction electrons and move with constant Fermi velocity, v_F.

2. An electron changes its direction (momentum) as a result of collision with other electrons, lattice vibrations, etc. Then each electron loses its memory of its direction of motion, so it moves as an independent classical particle randomly.

3. The spin of each electron is only very weakly coupled to the electron's orbital motion and it is unaffected by collision. However the weak spin-orbit coupling is taken into account in the relaxation time T_1. There is a probability $e^{-\frac{t}{T_1}}$ that the spin state will be undisturbed by collision during a time interval t.

Let $F(\mathbf{r}, r)$ denote the probability distribution for the position $\mathbf{r}$ of one electron at time t. If the time scale is much larger then mean collision time $\tau = \frac{\delta_\ell}{v_F}$, classical diffusion equation is valid

$$\frac{\partial F}{\partial t} = \frac{1}{3} v_F \delta_\ell \Delta F, \tag{2.39}$$

and the boundary condition is $\mathbf{n} \cdot \mathrm{grad} F = 0$ where $\mathbf{n}$ is the normal vector at any point of the metal surface. The ESR line shape is normally described as a function of parameters like spin susceptibility χ, spin relaxation time T_1, and g-factor. However in metals we need two extra parameters to get describe the line shape. The first is defined as $R = \sqrt{\frac{T_\mathrm{D}}{T_2}}$ where $T_\mathrm{D} = \frac{3\delta_\mathrm{Skin}^2}{2 v_F \delta_\ell}$ is the electron diffusion time across the skin depth. The second is T_T, the time it takes for the electron to diffuse through the whole sample. ESR spectroscopy measures the absorbed power in the sample by the so-called cavity perturbation technique. Therefore it is crucial to determine the power-frequency $P(\omega)$ function. Now we distinguish two different cases. The simpler one is when $T_\mathrm{T} << T_\mathrm{D}$, a thickness of the sample/film is smaller than the skin depth. The power absorbed is

$$P_a = \frac{\omega B_1^2 V \omega_0 \chi_0 T_2}{\mu_0 4 (1 + (\omega - \omega_0)^2 T_2^2)} \tag{2.40}$$

where V = volume of the sample, B_1 =amplitude of linearly polarized alternating magnetic field. This result totally independent of diffusion and gives Lorentz line with the half width $\frac{1}{T_2}$. The other case when $T_\mathrm{T} >> T_\mathrm{D}$ and $T_\mathrm{T} >> T_2$ is important for us. Taking into account the assumptions of Dyson the absorbed power (Fig. 2.8) is:

$$\begin{aligned} P_a = -\frac{1}{8}(\delta_\mathrm{Skin} \omega B_1^2 A \omega_0 \chi_0 T_2) R^2 \Bigg\{ & \frac{R^4(x^2-1) + 1 - 2R^2 x}{\mu_0[(R^2 x - 1)^2 + R^4]^2} \cdot \left(\frac{2\xi}{R(1+x^2)^{\frac{1}{2}}} \right. \\ & \left. + R^2(x+1) - 3 \right) + \frac{2R^2 - 2xR^4}{((R^2 x - 1)^2 + R^4)^2} \cdot \left(\frac{2\eta}{R(1+x^2)^{\frac{1}{2}}} + R^2(x-1) - 3 \right) \Bigg\} \end{aligned} \tag{2.41}$$

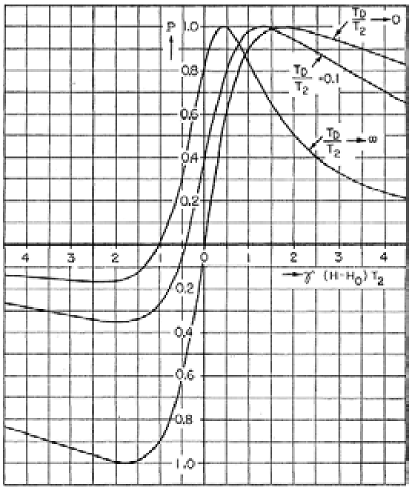

Figure 2.8: Absorbed power by ESR in thick metal films for different ratios of T_{D} and T_2 from Ref.[5]

where $x = (\omega - \omega_0)T_2$, $\xi = \mathrm{sign(x)}[(1+x^2)^{\frac{1}{2}} - 1]^{\frac{1}{2}}$, $\eta = [(1+x^2)^{\frac{1}{2}} + 1]^{\frac{1}{2}}$ and A is the surface of the sample.

The technical details of ESR signal detection is discussed later and we note that the magnetic field derivative of Pa is measured in ESR spectroscopy. It is readily obtained from Eq. (2.41) and shown in Fig. 2.9.

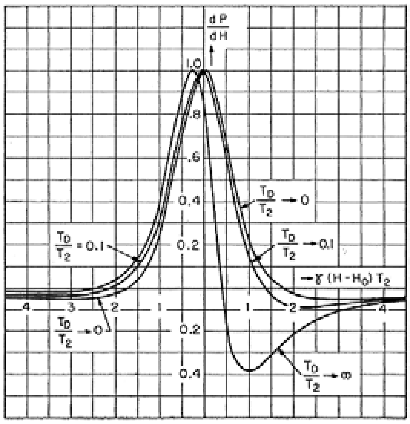

Figure 2.9: Derivative of power absorption from Ref. [5]

Knowing the $P(\omega)$ function, one can calculate T_{D} and T_2 by fitting the measured ESR signal.

2.3 Transmission Electron Spin Resonance and Spin Diffusion

There is some ambiguity in the ESR literature as to what is meant by transmission ESR [20]. There exist an ESR method when a single measuring cavity has an input and output coupling holes and the ESR signal is detected on the latter. In this thesis, we refer to transmission ESR (or TESR) by a method when two cavities are separated by a metallic film. The transmission occurs between the transmitting and receiving cavities bz means of the diffusing electrons which are excited in the earlier cavity.

In our case we have metallic samples and real transmission of conduction electrons in the sample. Electrons bring the non-equilibrium magnetization from one place to an other where they establish alternating electromagnetic field due to the precession of magnetization.Transmission of electrons through the sample happens according to the classical diffusion. If the spin relaxation time T_2 is long enough ($T_2 >> T_{\mathrm{T}}$) the excited spin state of the electron diffuses as well as the electron does. The transmitted signal of the diffusing electrons is detected in TESR in contrast to the conventional ESR when absorption due to the electrons near the surface is detected.

In 1957 Azbel', Gerasimenko and Lifshitz predicted selective transparency of metal films to microwaves at the resonant frequency of the conduction electron spins. They assumed energy transport because of diffusion of precessing conduction electrons through the metal [6]. Lewis and Carver were the first who observed such resonance transmission in lithium in 1964 [7]. A more detailed measurement was made by Schumacher and VanderVen [11]. They determined spin diffusion length by meausuring films with different thickness. They used the calculation of Kaplan instead of Azbel' et al. to prove their results [12]. Kaplan gave a new solution to electron spin resonance absorption using a modified Bloch equation[3]which includes diffusion:

$$\frac{d\mathbf{M}(t)}{dt} = \gamma[\mathbf{M} \times \mathbf{B}] - \frac{\mathbf{M}}{T_1} + D\Delta\mathbf{M}. \tag{2.42}$$

Now we follow the calculations and notations of Jánossy[17]: $D = \frac{1}{3}v_F^2\tau\left(\cos^2(\alpha) + \frac{\sin^2(\alpha)}{(\omega_c\tau)^2+1}\right)$ is diffusion constant, α is the angle of the magnetic field to the surface normal. $\omega_c = \frac{eB}{m*}$ is the cyclotron frequency where m* is the effective mass of the electrons, τ is the momentum collision time. The angle dependent part is near unity in our measurements. This calculation gives the relation between the magnetization and spin diffusion length at resonance:

$$M \sim e^{-\frac{d\sqrt{2}}{\delta_{\text{Diff}}}} \tag{2.43}$$

where $\delta_{\text{Diff}} = \sqrt{2DT_1} = \sqrt{\frac{2}{3}}v_F\sqrt{\tau T_1\left(\cos^2(\alpha) + \frac{\sin^2(\alpha)}{(\omega_c\tau)^2+1}\right)}$ is the spin diffusion length and d is the thickness of sample. Thus the transmitted power scales with this exponential factor.

The basic idea of measuring TESR signal came from Lewis and Carver. The lithium film were arranged so that they formed part of the common sidewall of two adjacent rectangular TE_{101} cavity. The incident power enters the

---

[3] Kaplan's calculation is closer to the formalism of common resonance calculation. Azbel' et al. and Dyson did not use Bloch equations.

first cavity called transmitter cavity, the other where we detect transmission signal is called receiver cavity. From the transmitter cavity we get the Dysonian line shape according to the traditional theory and experiment. Excited electrons diffuse through the skin-depth and the sample, keeping their spin state. The signal of the receiver cavity is approximately based on the rotating magnetization of the transmitted electrons from the skin depth of the other side as it is seen in Fig. 2.10.

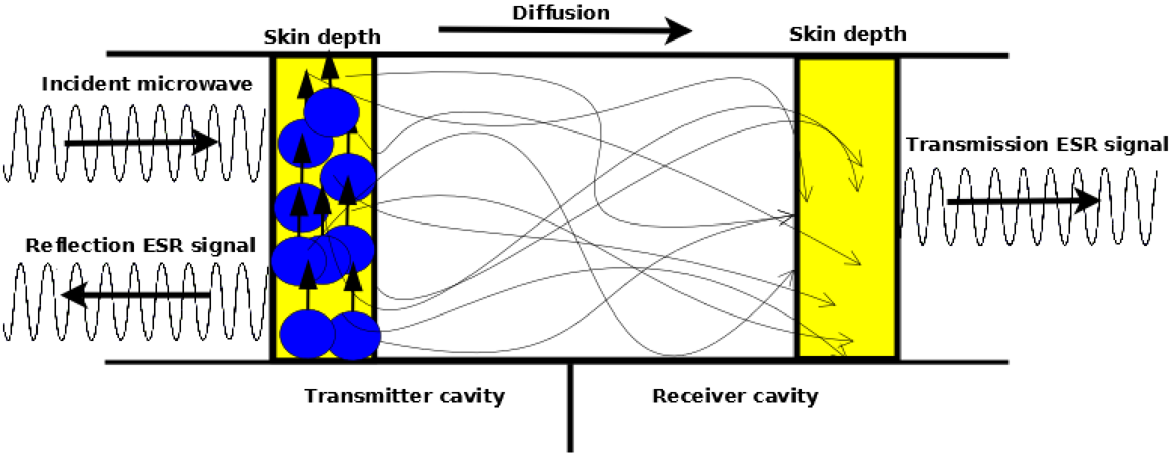

Figure 2.10: Schematics of transmission ESR.

VanderVen and Schumacher measured on lithium films with different thickness and they plotted relative transmitted signal considered sample thickness.

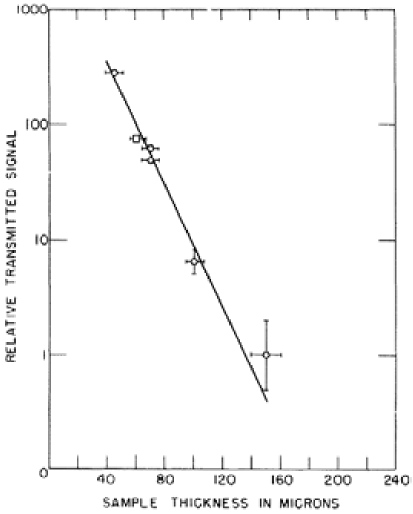

Figure 2.11: Signal vs. sample thickness on semilog plot [11].

The slope of the line scales with spin diffusion length which is $\delta_{\mathrm{Diff}} \approx 20\ \mu$m. The main goal of this master thesis is to reproduce this measurement with the appropriate spin diffusion length with a few improvements such as modulated ESR, low noise quadrature detection. The latter is possible due to the availability of low noise preamplifier (which were not available in the 1960's) and compact IQ mixer detectors.

Chapter 3

Results and discussions

In this chapter we discuss the steps which led us to TESR measurements. We give detailed discussion of quadrature ESR detection, cavity system, impedance matching and finally we calculate spin diffusion length of lithium from the measured spectra. Our intention was to reproduce an earlier TESR experiment on lithium with a modern instrumentation: the use of low noise microwave preamplifiers, IQ mixer detectors. In addition we employ magnetic field modulation which was not performed in the original experiments in Refs. [7, 11].

3.1 Conventional ESR with quadrature detection

We built a hybrid ESR microwave circuit by using of the commercial JEOL spectrometer and IQ mixer and Low Noise Amplifier. A photograph of the system is shown in Fig.3.1.

The JEOL spectrometer has a built-in AFC system which is employed herein. The 200 mW signal of the JEOL source is divided to provide the LO for the built-in mixer of the JEOL spectrometer and for the present IQ mixer, too. The ESR signal (RF) is also divided between the two mixers. This configuration allows to detect the IQ signal while the spectrometer's AFC is working properly. A block diagram is shown in Fig. 3.2.

We performed measurement on an ESR standard: DPPH.

In the measurement we get derivative of absorptional signal (proportinal to χ'') and derivative of dispersive signal (proportinal to χ'). To check the validity of the use of the IQ detection, we perform a numerical Kramers-Kronig traonsformation (which is called discrete Hilbert transform) of the absorption signal to obtain the numerical dispersion signal. The lines do not go exactly to zero and there is a little difference between the measured and calculated dispersion line. The reason is some offset problem and imperfection of mixer LO port. Probably there is not an exact 90° difference between the I and Q

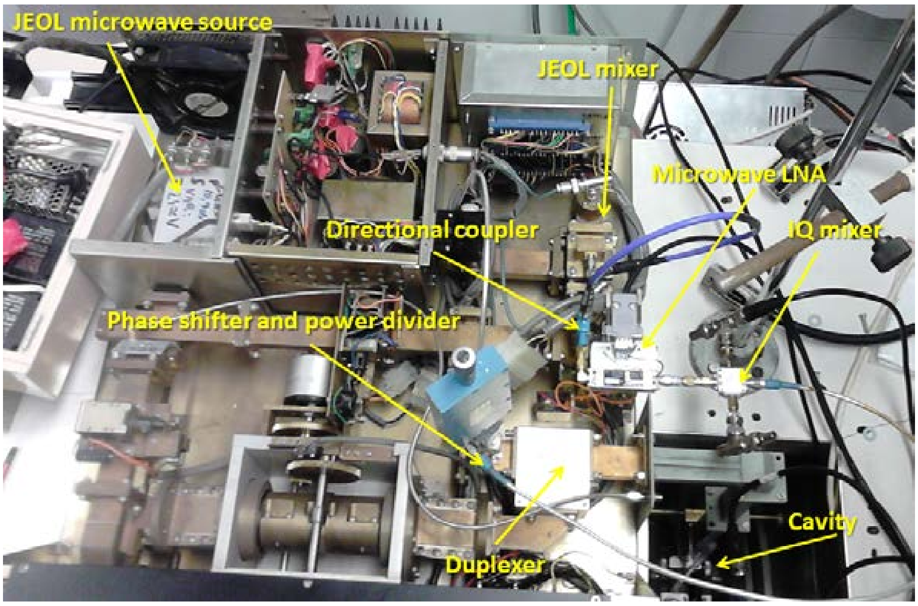

Figure 3.1: The microwave bridge of the ESR spectrometer with an IQ mixer.

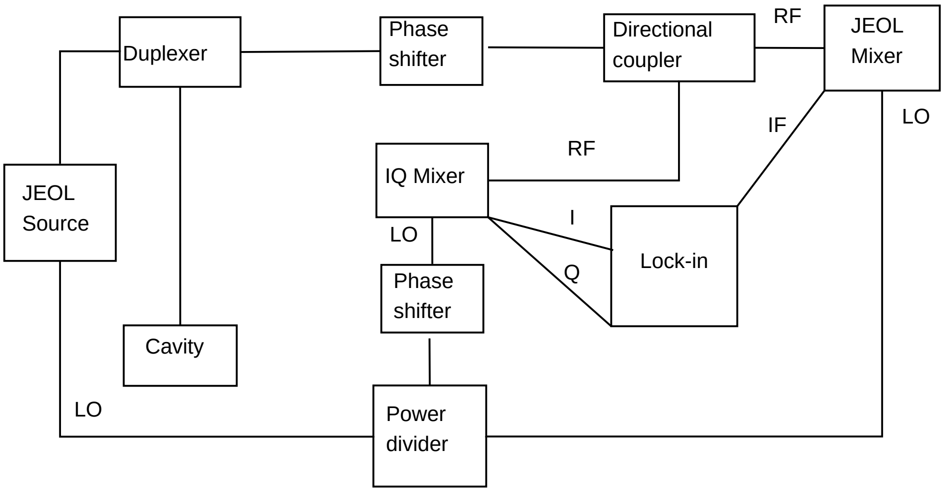

Figure 3.2: Schematics of the quadrature detected ESR.

ports.

There is varying sign convention considering χ'' in the scientific literature. Slichter uses a $\chi = \chi' - \mathbf{i}\chi''$ form for dynamic susceptibility, Wilmshurts uses $\chi = \chi' + \mathbf{i}\chi''$. That is why Fig.3.4 is rotated by 90° from Fig.2.6. In Fig.3.4, we plot χ' vs. χ''. Ideally this should form a circle which crosses the origin for $\omega = \pm\infty$. We see in Fig.3.4 and in Fig.3.3 that we have Kramers-Kronig pairs, we are in the range of linear response, and the IQ mixer works well. This also shows that the use of the IQ mixer could be advantageous for the TESR experiment.

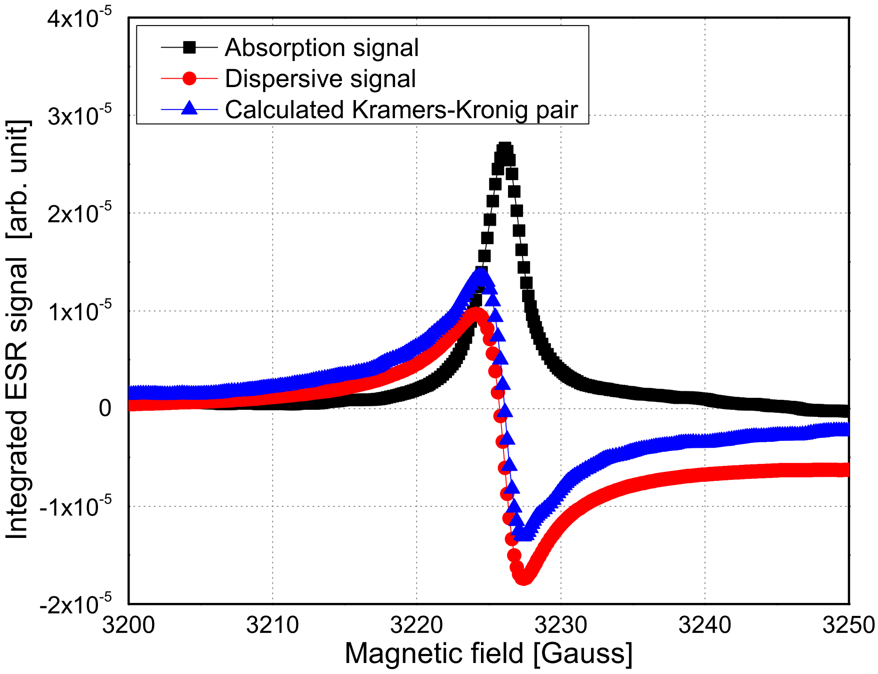

Figure 3.3: Integrated ESR signals from I and Q output and the calculated Kramers-Kronig pair of the absorption.

3.2 The transmission ESR system

The most important part of the TEST system is the two coupled cavities. Its construction is therefore introduced first. Then we introduce the characterization methods of the TESR system.

3.2.1 Parameters of the cavity

In TESR measurement geometry of the cavity is limited in comparison with conventional ESR cavity. At first we need two cavities, and we need proper microwave mode to have perpendicular $\mathbf{B}_1$ field to $\mathbf{B}_0$ at the sidewall which joins the two cavities. Following the first articles of TESR we use rectangular cavity with TE_{101} mode.

In this geometry in Fig.3.6 we overlook electron drift by electric field because this motion is in-plane. Thus plane perpendicular motion is based on only diffusion effect.

Lithium is air-sensitive hence we have to construct a cavity system which is air tight. A vacuum closed cavity would be difficult to build but it is not neccessary. We have an MBraun GloveBox (dry box) and we commission the

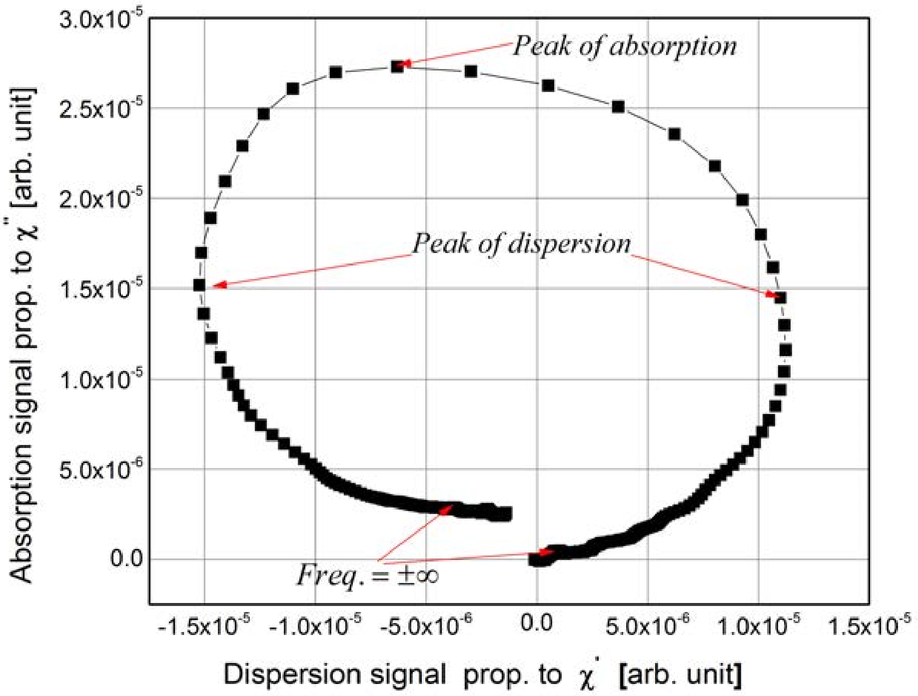

Figure 3.4: The circle diagram of dispersion and absorption signal measured for DPPH with the IQ mixer. The theoretical curve for this type of measurement is shown in Fig. 2.6.

cavity system inside it. As a result, the cavity is filled with argon and is sealed by o-rings and mylar foil shown in Fig. 3.7.

In the first TESR measurements lock-in technique was used so modulated signal was required. The microwave intensity was modulated with PIN diodes. As a modification to the previous TESR works, we apply magnetic field modulation rather than microwave intensity modulation (chopping). It has two advantages: it allows the simultaneous measurement of the signal reflected from the first cavity and the transmission signal. The reflection signal cannot be measured when microwave intensity is chopped as it interferes with the AFC. The second advantage is that the magnetic field modulation selects the microwave intensity in the second cavity which is transmitted through the sample. It is insensitive to the leakage microwaves.

3.2.2 Sample preparation

For TESR measurements we need lithium films with thicknesses of a few hundreds μm. We used lithium granules and we smashed and stretched them to obtain thin films. We place the film between two copper plates. In the middle of the copper plate there is a hole where the sample is placed. We put some lithium film on the surface of the copper plate which is in contact with the surface of the cavity in order to get good plumbing and to avoid microwave leakage.

There are two requirements for the construction of the transmission cavity system. Namely, the air tight composition and the reduction of microwave leakage between the cavities. The first requirement is fulfilled with the use of o-rings and vacuum grease. However it does not matter how strong we join two cavities, we experience some leakage power in the second cavity[1] from the first one. Having the sample between the cavities, the leakage is about 50-60 dB. It gives us a a lower limit for the magnitude of the TESR signal. Namely, the sample inside the first cavity radiates an ESR signal (which is also magnetic field modulated) which is not related to the TESR signal but enters the second cavity in any case together with the leakage. This means no TESR signal can be observed which is smaller than 60 dB of the ESR signal inside the first cavity. Transmission signal scales with the factor of $e^{-\frac{d}{\delta_{\text{Diff}}}}$. In practice if the sample has more than 250-300 μm thickness we observe only the leakage signal in the receiver cavity. We performed several experiments that this leakage comes from only the joint of two cavity and not from the joint of the flanges or waveguides. Another limitation occurs together with the leakage: an unmodulated (or DC) microwave signal enters the second cavity which does not affect the lock-in measurement, however it can saturated the LNA before the mixer or the RF port of the mixer itself. To hand this power, we always checked that the LNA works outside saturation and also that the mixer is not saturated either.

3.2.3 Characterization of the TESR system

In order to characterize our system we made several control experiments. The very first experiment was on DPPH. We put the sample inside the cavity system but we place an o-ring and separation copper plate with hole between two cavity. Diameter of hole is the same as the coupling plane. We detect both signals; from the transmitter cavity in reflection and from the receiver cavity in transmission. We found that both ESR signal is in the same order of magnitude if both cavities are critically coupled. It means that our cavity design is symmetric.

Other measurement was about leakage. We had to make the following measurements before every TESR experiment in order to determine resonance frequency of the cavity, Q factor, and leakage power. Now we discuss an ideal case when there is no sample but only a copper plate with no holes between the cavities. We determine resonant frequencies and Q factor with the so-called Cavity Sweep method. Then we measure leakage power with a modified Cavity

---

[1] This problem is symmetric that is why no use to differentiate transmitter and receiver cavity.

Sweep method as shown in Fig.3.11.

We sweep the frequency and we measure the reflected power from the transmitter cavity. When we find the resonant frequency of the cavity we measure zero reflected power as it is critically coupled. We record the reflected curve and we fit a Lorentz curve shown in Fig.3.12.

The curve of receiver cavity is quite similar except the resonance frequency which can be somewhat different (up to 40 MHz) and the Q factor can be different, too.Although the two cavities were manufactured to have the same length and cross section, their parameters are not the same. To join every part of the cavity system properly is technically difficult which results in the difference of the parameters. This problem is present in every configuration of transmission cavity system.

The leakage is determined in a different configuration as shown in Fig.3.13.

We sweep the frequency and we detect transmitted signal from the receiver cavity. This signal power is much lower than the reflected signal that is why we have to amplify it.

In Fig.3.14 the peaks correspond the resonance frequency of the corresponding cavity. Leakage is calculated from voltage-power characterization of the detector. 79.9 dB was the smallest leakage we detected. Normally, with lithium sample the leakage is about 60 dB. If the expected transmission signal is the order of the leakage we cannot measure it. As a result of the substantial leakage, we follow a different route from the previous approaches, where much lower (up to 180 dB) leakage were attained. We measure the magnitude of the TESR signal and compare it to the ESR signal which is reflected back from the transmitting cavity. This way the TESR signal is accurately calibrated. The arrangement of reflection ESR measurement shown in Fig.3.15.

3.3 Transmission ESR results on lithium

We prepared four lithium samples with different thickness. Sample with 90 μm and 150 μm thickness were prepared as we mentioned in the previous section. Because of technical reasons, the thicker samples were wider and longer thus they covered the whole cross section of cavity and we did not use sample holder. We measured the reflection and transmission ESR signals with the IQ mixer for every sample. The ESR intensity contains the adequate information so there is no specific microwave phase adjustment. We obtained the curves like in Fig. 3.16 for every thickness.

The incident power were 20 dBm but in reflection ESR measurements we had to attenuate the power because of the because of the not optimal isolation of the duplexer (a microwave circulator). We calculated the resulting intensity (T,R) of TESR and reflection ESR from the peak-to-peak I and Q voltages.

$$\mathrm{T\backslash R} = \sqrt{\mathrm{I}^2_{\mathrm{T\backslash R}} + \mathrm{Q}^2_{\mathrm{T\backslash R}}} \tag{3.1}$$

Thus the intensity is proportional to the microwave voltages. We measured the cavity resonance and leakage before every TESR experiment. In the leakage measurements we found that there are two resonant frequency[2] with different leakage. We measured on that frequency which had smaller leakage. In this case the impedance were not matched perfectly between the two cavities. In Appendix A we show that it is not so disturbing effect.

As it is shown in Fig.3.17 where the leakage is higher than the expected signal at 480 μm, we are not able to measure TESR. We fitted a line according to the following equation:

$$20\log\left(\frac{T}{R}\right) = 20\log\left(Ce^{-\frac{d}{2\delta_{\mathrm{D}}}}\right) \tag{3.2}$$

$\delta_D = v_F\sqrt{\frac{1}{3}\tau T_1}$ is the effective spin diffusion length. The intensities are proportional to the microwave voltage thus factor of two in the exponent comes from the general relation between power and voltage $\sqrt{P} \sim U$. C is an empirical constant. We chose $C = 1$ in the theoretical curve. In this curve $T_1 = 10^{-7}$ s, $v_F = 1.3\cdot 10^6 \frac{\mathrm{m}}{\mathrm{s}}$, $\tau = 8.462\cdot 10^{-15}$ s and they give $\delta_{\mathrm{D}} = 21.8$ μm according to the calculation of Schumacher and VanderVen [11]. They measured $\delta_{\mathrm{D}} = 22.6$ μm. Our fitted line gives $\delta_{\mathrm{D}} = 22.1$ μm. Although the measured result is quite close to the publicated one, there is a huge uncertanity considering τ and T_1. We do not know the concentration of impurities of our lithium films. The agreement between the experimental result and the theoretical curve confirms that we did observe the TESR signal in lithium.

3.3.1 The validity of the Kramers-Kronig pairs in quadrature detected TESR

We measured the I and Q signals of TESR and ESR measurements with an arbitrary phase. The signals are proportional to the derivative of dynamic spin susceptibility with respect to ω. The arbitrary phase ϕ causes the mixture of absorption and dispersive susceptibilites in I and Q. I and Q signals are still perpendicular.

$$I \sim \cos(\phi)\frac{\mathrm{d}\chi'(\omega)}{\mathrm{d}\omega} + \sin(\phi)\frac{\mathrm{d}\chi''(\omega)}{\mathrm{d}\omega} \tag{3.3}$$

$$Q \sim -\sin(\phi)\frac{\mathrm{d}\chi'(\omega)}{\mathrm{d}\omega} + \cos(\phi)\frac{\mathrm{d}\chi''(\omega)}{\mathrm{d}\omega} \tag{3.4}$$

Considering some basic properties of the Hilbert transform we prove that Q signal is the Hilbert transform of I signal, consequently we measured a Kramers-Kronig pair and ESR and TESR both satisfy the linear response theory.

---

[2] The tunable cavity was not ready by that time.

H indicates the Hilbert transform, $g(t)$ is a signal, $\mathrm{H}[g(t)]$ is the transformed signal, t is a general variable.

$$\mathrm{H}[g(t)] = \frac{1}{\pi}\int_{-\infty}^{\infty}\frac{g(\tau)}{t-\tau}\mathrm{d}\tau = \frac{1}{\pi}\int_{-\infty}^{\infty}\frac{g(t-\tau)}{\tau} \tag{3.5}$$

$\mathrm{H}[g(t)]$ is the convolution of $\frac{1}{\pi t}$ with the signal $g(t)$ [18]. The Hilbert transform is linear from the fact, that the Hilbert transform is the output of a linear system, then

$$\mathrm{H}[ag(t) + bh(t)] = a\mathrm{H}[g(t)] + b\mathrm{H}[h(t)] \tag{3.6}$$

where a and b are arbitrary complex numbers. Other important property is that Hilbert transform of the derivative of a signal is the derivative of the Hilbert transform.

$$\mathrm{H}\left[\frac{\mathrm{d}g(t)}{\mathrm{d}t}\right] = \frac{\mathrm{d}}{\mathrm{d}t}\mathrm{H}[g(t)] \tag{3.7}$$

According to Leibniz's Integral Rule

$$\frac{\mathrm{d}}{\mathrm{d}c}\int_{a}^{b} f(x,c)\mathrm{d}x = \int_{a}^{b}\frac{\partial f(x,c)}{\partial c}\mathrm{d}x \tag{3.8}$$

if a and b are not the function of c. In our case a and b are definite. Now

$$\begin{aligned}\frac{\mathrm{d}}{\mathrm{d}t}\mathrm{H}[g(t)] &= \frac{\mathrm{d}}{\mathrm{d}t}\frac{1}{\pi}\int_{-\infty}^{\infty}\frac{g(t-\tau)}{\tau}\mathrm{d}\tau \\ &= \frac{1}{\pi}\int_{-\infty}^{\infty}\frac{g'(t-\tau)}{\tau}\mathrm{d}\tau \\ &= \mathrm{H}[g'(t)]\end{aligned} \tag{3.9}$$

where $g'(t) = \frac{\mathrm{d}g(t)}{\mathrm{d}t}$.

There is a slight difference among (2.17),(2.18) and Hilbert transform. The integration goes with the first term of denominator in formulas of Kramers-Kronig but in Hilbert transform it goes with the second term. The result reads: $\mathrm{H}[\chi''] = -\mathrm{H}[\chi']$ and $\mathrm{H}[\chi'] = \mathrm{H}[\chi'']$. The Hilbert transform of I is:

$$\begin{aligned}\mathrm{H}[I] &\sim \mathrm{H}\frac{\mathrm{d}}{\mathrm{d}t}(\cos(\phi)\chi' + \sin(\phi)\chi'') \\ &\sim \frac{\mathrm{d}}{\mathrm{d}t}(\cos(\phi)\mathrm{H}[\chi'] + \sin(\phi)\mathrm{H}[\chi'']) \\ &\sim \frac{\mathrm{d}}{\mathrm{d}t}(-\sin(\phi)\chi' + \cos(\phi)\chi'') \\ &\sim Q\end{aligned} \tag{3.10}$$

where χ' and χ'' are ω dependent functions.

The OriginLab program calculated the discrete Hilbert transforms of the signals. In Fig. 3.18 we show that the IQ mixer works properly and linear response theory is still valid.

3.3.2 Control experiment

Although we measured the direct leakage with a modified Cavity Sweep method, we performed additional control experiments. We placed a DPPH sample (less than 0.2 mg) next to the lithium sample which had about 150-200μm of thickness.The idea of the control experiment was to place an additional ESR sample (DPPH) into the transmitter cavity. If we indeed observe the TESR of lithium, the ESR signal of the DPPH should be suppressed by the amount of the leakage in the receiver cavity, whereas the TESR signal of lithium is expected to be much larger. The result is shown in Fig. 3.19.

The g-factor of DPPH is 2.0036, its resonance occurs at lower magnetic fields. The g-factor of lithium is very close to the free electron g_e-factor 2.0023 ,$|g_e - g_{\mathrm{Li}}| = 2 \cdot 10^{-6}$ [19]. The linewidth is about 2 Gauss for both samples. We had to diminish the modulation amplitude because higher amplitude leads total overlap of the lines. Therefore we got very low intensity lithium signals in reflection. We measured 63 dB direct leakage and the DPPH intensity decreased with this factor in transmission measurement. Lithium intensity decreased with 38 dB. This experiment confirms the earlier assignment, i.e. that we observe TESR of lithium. Some leakage is present but its magnitude is controlled and its effect is taken into account.

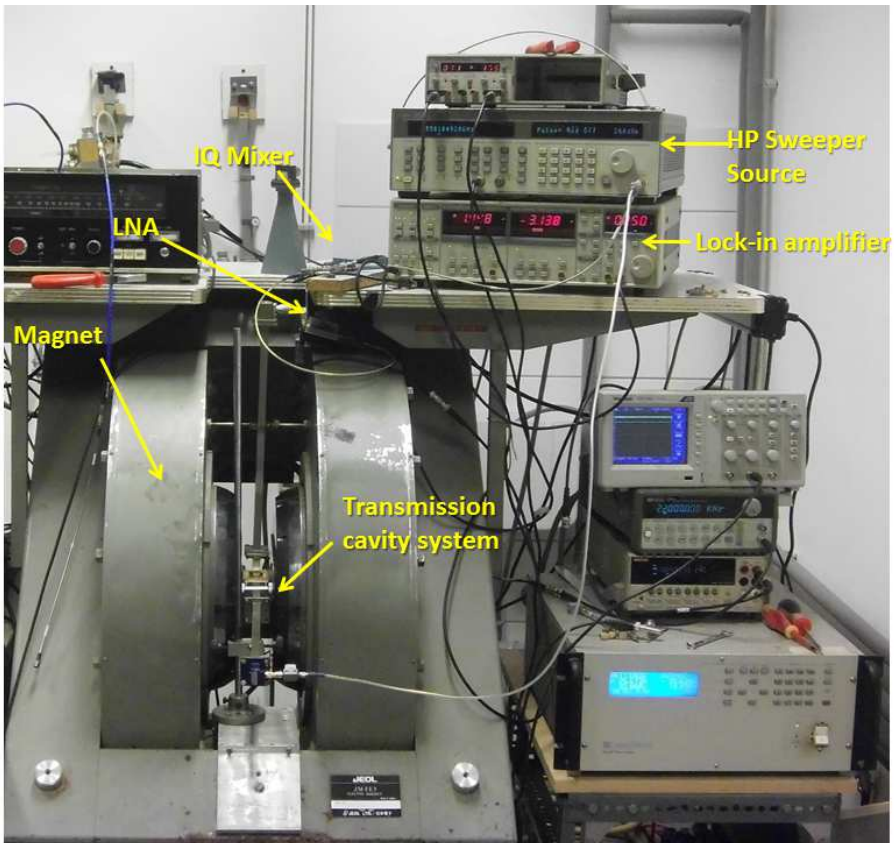

Figure 3.5: Photo of the measurement setup.

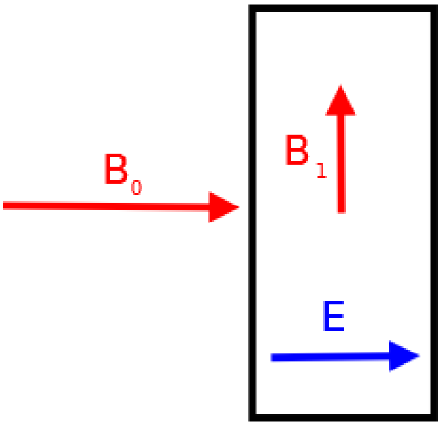

Figure 3.6: Directions of electric and magnetic fields between two cavities where the sample is placed. Vectors are in the plane of lithium film.

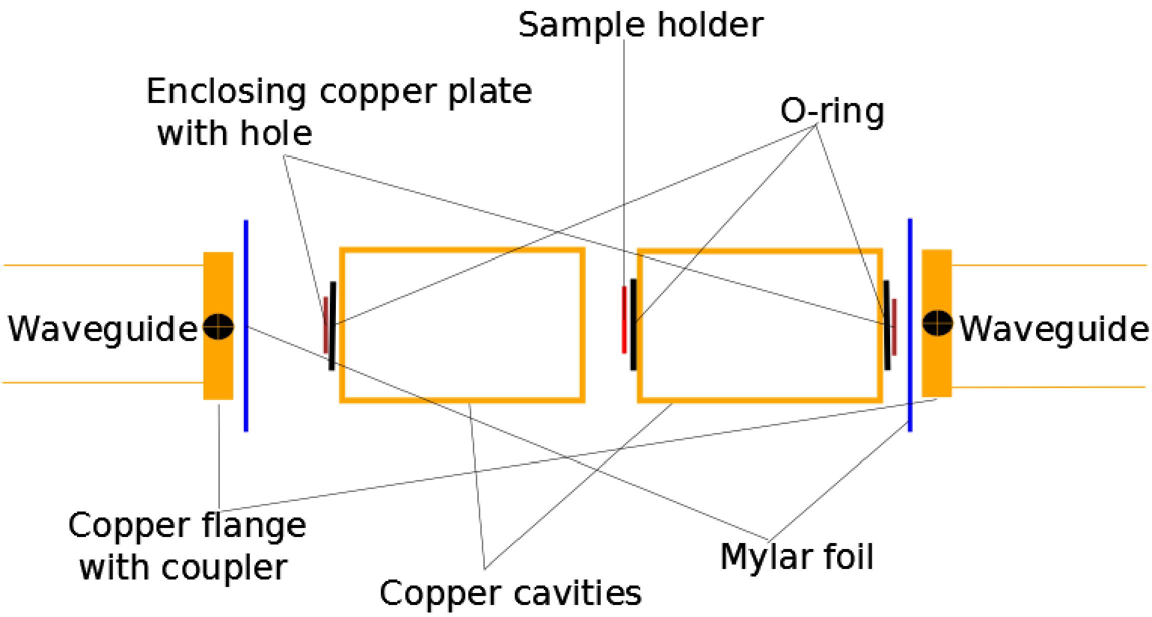

Figure 3.7: Schematics of transmission cavity system.

Figure 3.8: The assembled transmission cavity system. Four holes on the top are for the modulation coil.

Figure 3.9: Sample and sample holder photographed inside the glovebox.

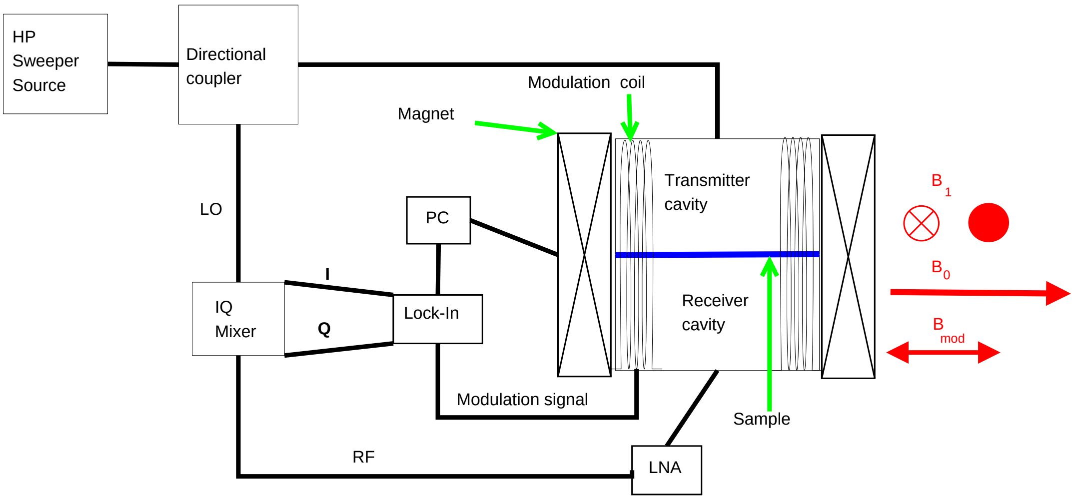

Figure 3.10: Schematics of TESR spectrometer

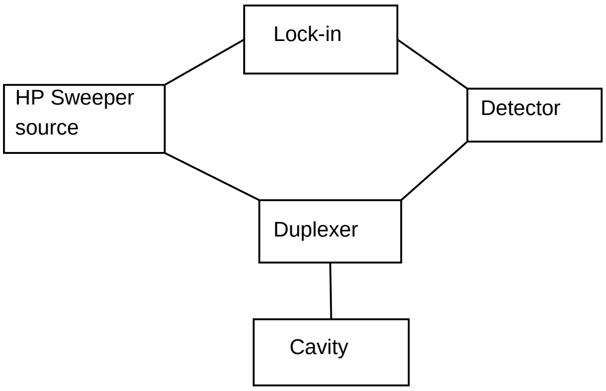

Figure 3.11: Schematics of Cavity Sweep arrangement

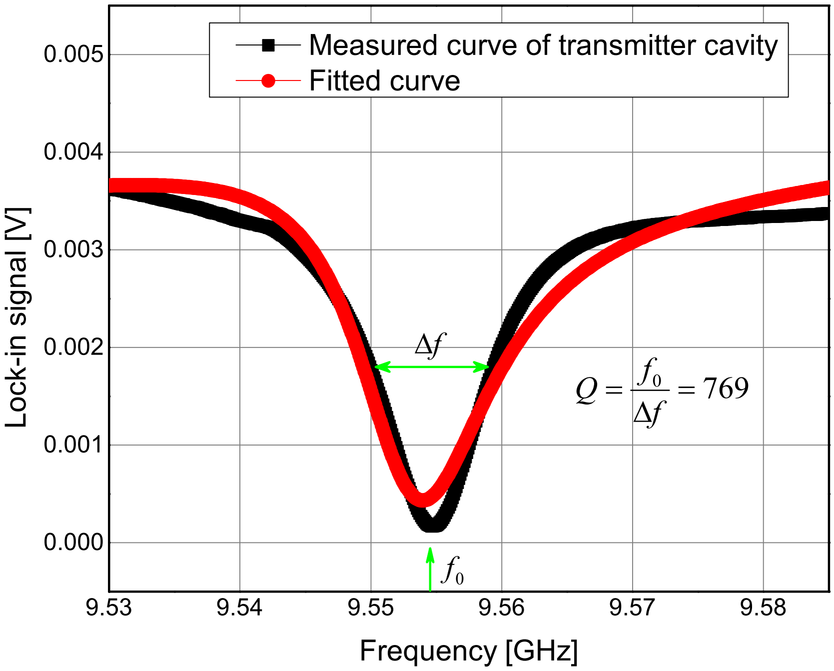

Figure 3.12: Cavity sweep of transmitter cavity. The fitted curve is a Lorentzian function

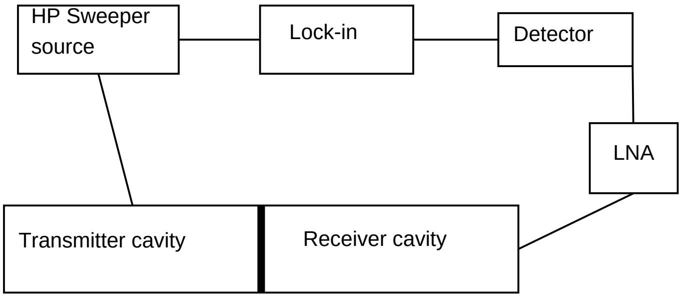

Figure 3.13: Schematics of modified Cavity Sweep arrangement which is used to measure the amount of leakage.

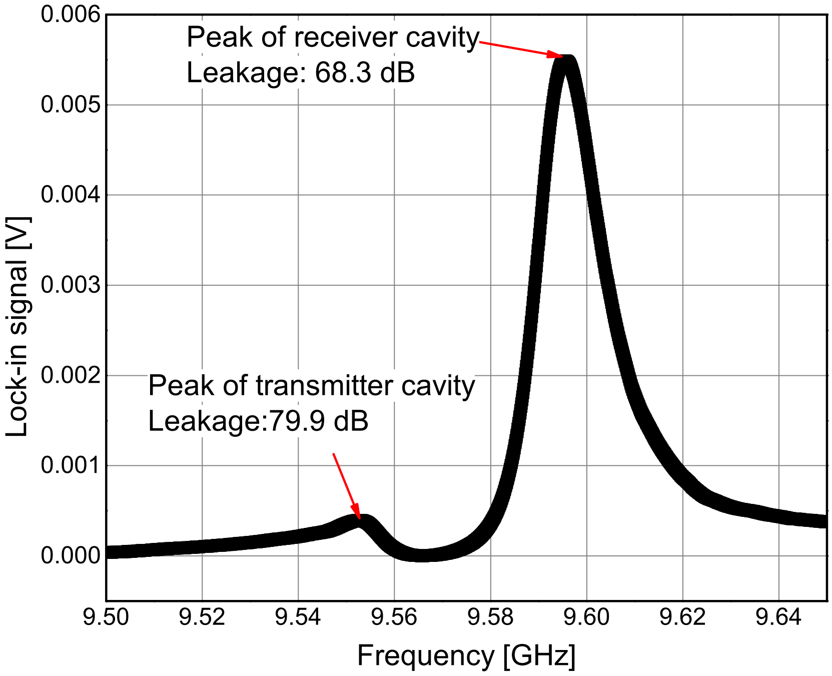

Figure 3.14: Crosstalk characterization with modified Cavity Sweep.

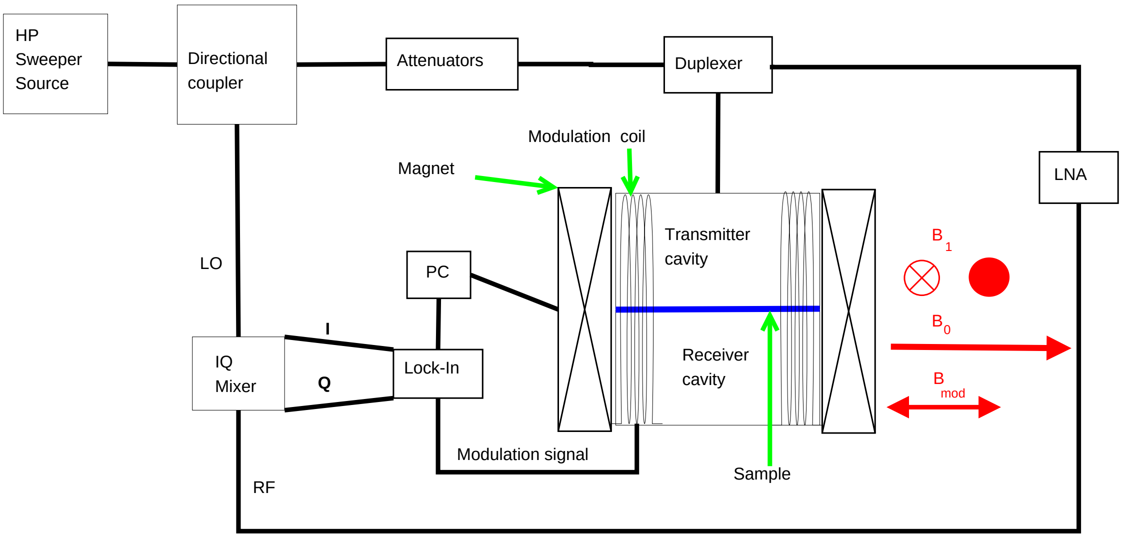

Figure 3.15: Schematics of ESR spectrometer for reference signal measurement.

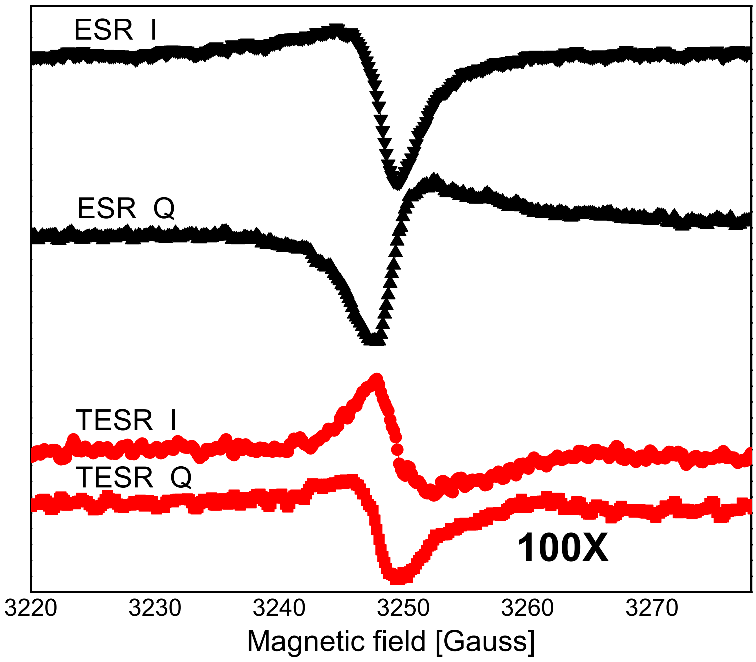

Figure 3.16: Detected signals measured on 200μm film. The microwave phases are random. TESR signal is multiplied by 100 for better visibility.

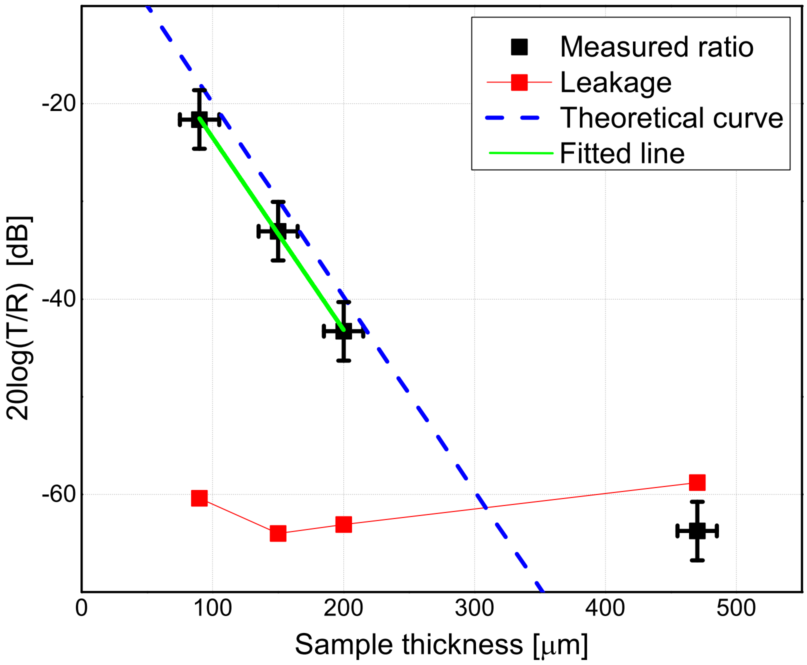

Figure 3.17: Relative transmission signal and leakage with respect to the sample thickness. The leakage is shown for comparison. A dashed curve shows the theoretically expected relative TESR signal.

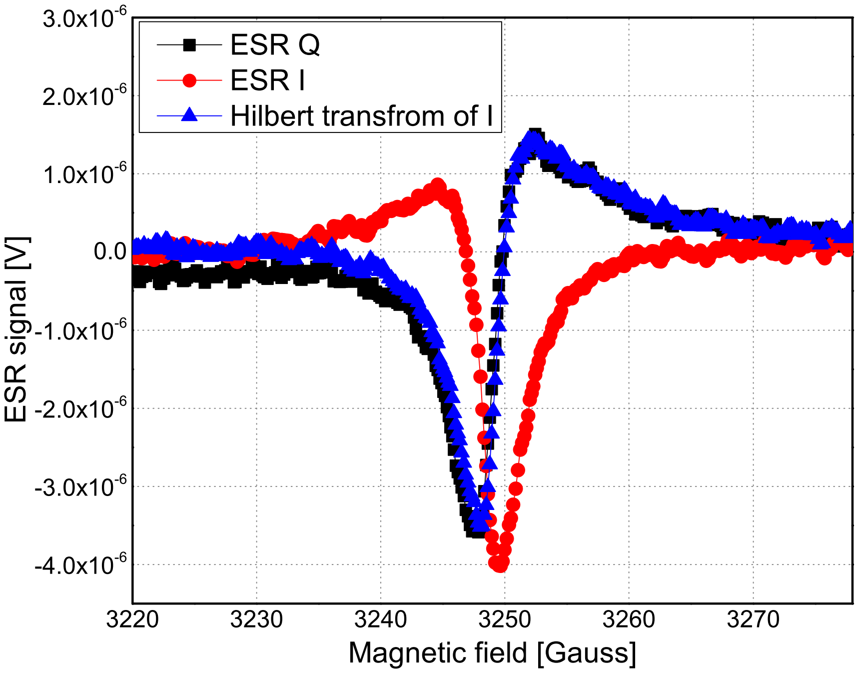

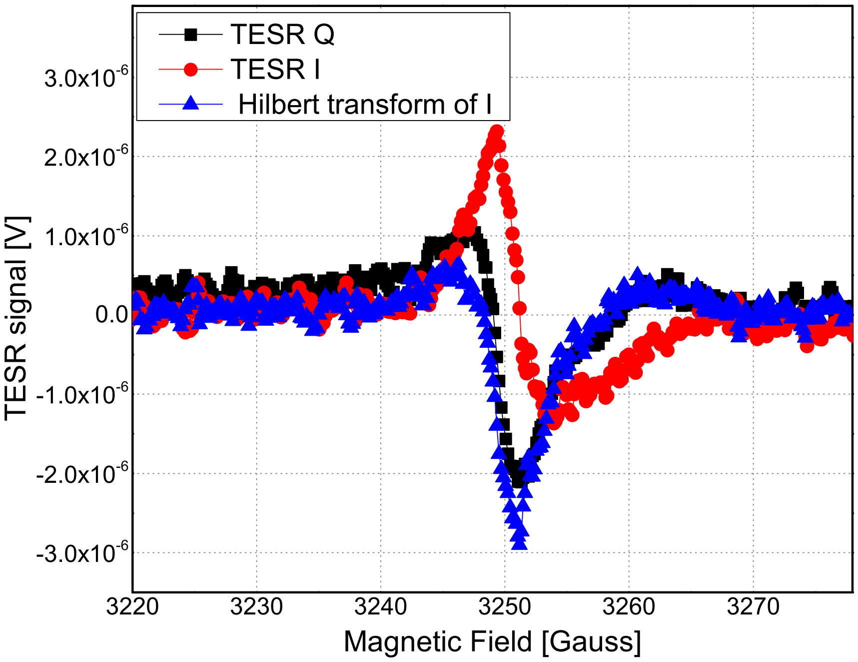

Figure 3.18: The IQ mixer signals of the 200 μm sample and Hilbert transforms.

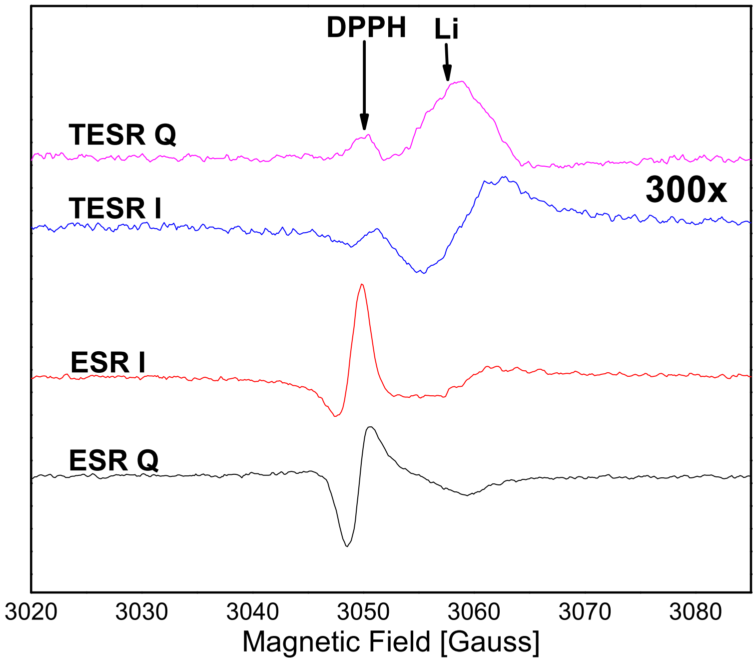

Figure 3.19: Detected signals measured on DPPH and lithium film for the receiver cavity, i.e. in transmission (upper two curves) and for the transmitter cavity in reflection (lower two curves). The microwave phases are arbitrary. The TESR signal is multiplied by 300 for better visibility. Signal at lower field is DPPH.

Chapter 4

Summary

In this master thesis we summarized the technical and theoretical background of electron spin resonance and profoundly understood the features of detected signals. We improved a transmission cavity system and an appropriate microwave circuit for detecting low level signals. Transmission electron spin resonance measurement was performed with modern devices and we showed how effective they worked. The TESR spectroscopy has great opportunities in spintronics because the simultaneous detection of transport and spectroscopic phenomena is possible.

Future plans are to measure TESR on alkali doped graphite and to develop a pulsed ESR with this transmission cavity system with which even pure graphene becomes measurable.

Appendix A

Impedance matching

Impedance matching is a general term which has important role when when we join two different element of a circuit(waveguides, cavities, detectors, PIN diodes etc.) Now we give a simple idea of impedance matching then we explain how we match the transmission cavity system.

If we have DC circuit the load gets the maximum power when the impedance of the load equals the impedance of the source $Z_{\mathrm{S}} = Z_{\mathrm{L}}$ and $P_{max} = \frac{U_{\mathrm{S}}^2}{4Z_{\mathrm{L}}}$.

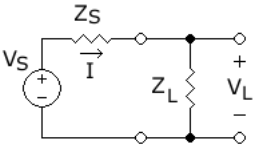

Figure A.1: Circuit model of a source attached to a load from Ref. [23]

In an AC circuit the previous thoughts are valid but for the maximum power the $Z_{\mathrm{S}} = Z_{\mathrm{L}}^*$ is necessary where * indicates the complex conjugate. The perfect impedance matching means that the reflected signal(power or voltage) is zero. In general case the source can be a line which is matched to a different line (which is the load) or a cavity which is matched to a waveguide or to an other cavity. If there is no perfect impedance matching we can observe reflection resulting standing waves that cause noise or false results in measurements. Theoretical background of the reflection is discussed in *telegrapher's equations* which come from Olivier Heaviside. Reflection coefficient Γ is used to characterize the reflection of the mismatched components. Γ is the ratio of complex amplitude of the reflected signal to that of incident signal. In transmission line the signal is the electric field strength (E) which correspond the voltage (U)

$$\Gamma = \frac{Z_{\mathrm{L}} - Z_{\mathrm{S}}}{Z_{\mathrm{L}} + Z_{\mathrm{S}}} = \frac{E_{\mathrm{in}}}{E_{\mathrm{refl}}} = \frac{U_{\mathrm{in}}}{U_{\mathrm{refl}}}. \tag{A.1}$$

For a rectangular cavity the impedance is

$$Z = \frac{k\sqrt{\frac{\mu}{\epsilon}}}{\sqrt{k^2 - \left(\frac{\pi}{a}\right)^2}} \tag{A.2}$$

where a is the length of longer side of the cross section of the waveguide, $k = \omega\sqrt{\mu\epsilon}$, μ and ϵ are the total permeability and permittivity respectively, ω is the cavity resonance angular frequency [21, 22].

Every TESR measurement on different samples requires a reconstruction of the cavity system. We observed that the resonance frequency of the transmitter and receiver cavity had different values from experiment to experiment. This effect was probably related to the way the cavity wall-end copper plate was mounted. Now we show that the different resonance frequency and impedance does not cause significant effect on the experiments. Table A.1 shows that reflection coefficient much less than unity therefore it has no effect on the transmission ESR signal. The lithium sample behaves as an radiant source. In the receiver cavity the diffusing electrons are able to build up the microwave field with the resonance frequency of the transmitter cavity.

Sample size [μm]	Δf [MHz]	Γ
90	30.619	0.001336
150	27.101	0.001265
200	250.638	0.01088
480	378.43	0.01647

Table A.1: Reflection coefficient with respect to the frequency difference between transmitter and receiver cavity.

A.1 Tests of impedance matching

We made a tunable receiver cavity[1] and we examined the leakage of the transmission cavity system when only a holeless copper plate was placed between the cavities.

Fig. A.2 shows that the leakage power add up when the two cavities are brought to a common resonance frequency. This also means that a slight detuning between the two cavities do not affect neither the leakage nor the TESR signal.

In other experiment we removed the enclosing copper plate of the receiver cavity. The receiver cavity and the transmitter waveguide are totally impedance mismatched in this case. A 80 μm thick lithium film was placed after the transmitter cavity. The result is shown in Fig.A.3.

---

[1] This construction was not properly air tight so it had a limited use in the TESR experiments.

Herein the TESR signal was decreased as we expected according to the inappropriate impedance matching. Direct leakage remained the same.

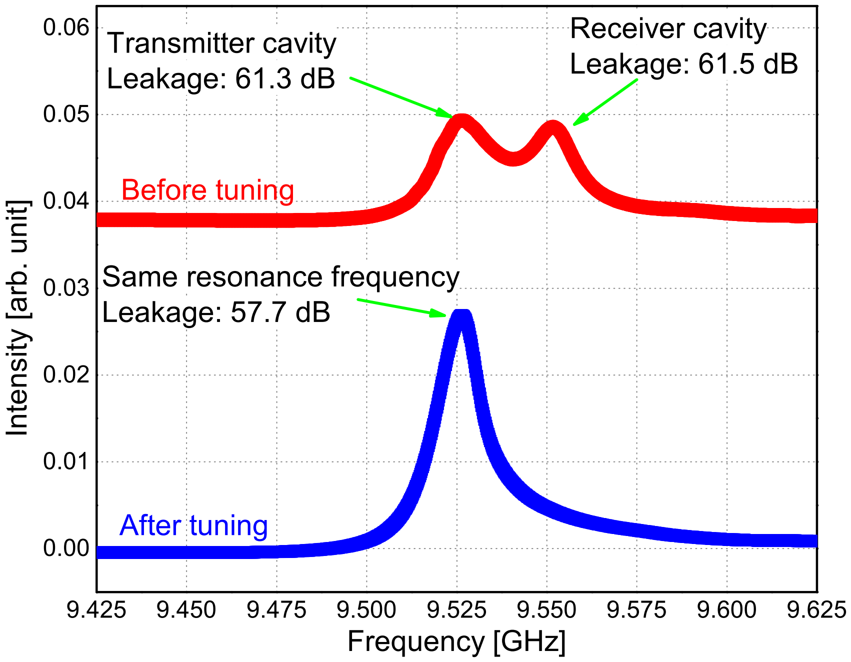

Figure A.2: Modified Cavity Sweep on tunable cavity system

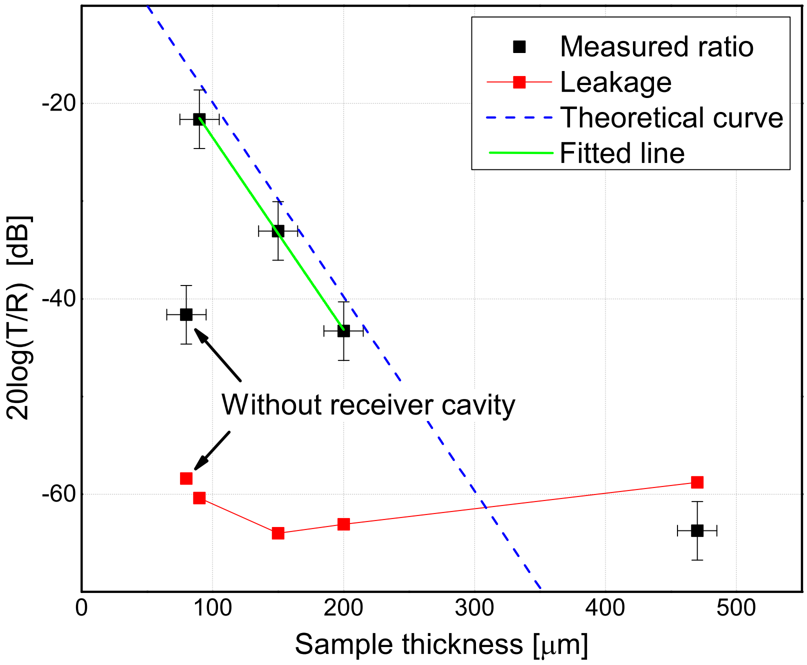

Figure A.3: The original measurement results with the results of one cavity measurement.

Appendix B

Technical details of the TESR spectrometer

B.1 Cavity parameters

The first articles of TESR experiments used a TE_{101} mode cavity. This is advantageous because at the end of the cavity,the magnetic field is finite. The electric field is only along to y axis, so is does not cause drift current along to z axis as shown in FigB.1.

Standing waves inside the TE_{101} cavity are described as:

$$H_z = \mathbf{i}\frac{\pi E_0}{k\eta a}\cos\left(\frac{\pi x}{a}\right)\sin\left(\frac{\pi z}{d}\right) \tag{B.1}$$

$$H_x = -\mathbf{i}\frac{\pi E_0}{Z}\sin\left(\frac{\pi x}{a}\right)\cos\left(\frac{\pi z}{d}\right) \tag{B.2}$$

$$E_y = E_0\sin\left(\frac{\pi x}{a}\right)\sin\left(\frac{\pi z}{d}\right) \tag{B.3}$$

where $\eta = \sqrt{\frac{\mu}{\epsilon}}$, Z is the impedance of the cavity, $\mathbf{i} = \sqrt{-1}$, and $k = \omega\sqrt{\mu\epsilon}$. The resonant frequency is

$$f_{101} = \frac{c}{2\pi\sqrt{\mu_r\epsilon_r}}\sqrt{\left(\frac{\pi}{a}\right)^2 + \left(\frac{\pi}{d}\right)^2} \tag{B.4}$$

. We made the simplest matching to the general X-band waveguide wherein $a = 23.3$ mm, $b = 10$ mm, so the size of cross section of the cavity and the waveguide are the same. We chose 9.5 GHz for resonance frequency which gave $d = 21.44$ mm. We constructed the transmitter and receiver cavity with the same parameters. The resonance frequency depends on the geometric parameters of the cavity and on the material filling the cavity. The common solution for tuning a cavity is to change the filling material. We used a plastic screw as a tuner which penetrated the cavity.

To obtain critical coupling which means perfect impedance matching, we put a metal coupler into the flange which presses the o-ring and the cavity as shown in Fig. B.2.

Several experiments showed that the most effective coupling is reached when the coupler is parallel to the electric field, and the coupler is placed where the electric field has maximum value ($x = \frac{a}{2}$).

The best size of the hole of enclosing copper plate was determined by experimental way. We closed the cavity with different plates which had 3-10 mm diameter holes and we performed Cavity Sweep. We chose the plate which had diameter 6.5 mm because it gave critical coupling and high Q-factor. The hole of the sample holder had 6.5 mm diameter as well.

B.2 TESR experiment parameters

The output of the microwave source was always 20 dBm. The reflection ESR measurement was performed with at least 40 dB attenuation of the source power. Less attenuation caused the saturation of the IQ mixer. The reason is the imperfection of the duplexer: it is a circulator which has isolation of about 30 dB, i.e. some of the exciting power always reaches the mixer as shown in FigB.3.

If we used 20 dBm power, the leakage signal at RF port would be -30 dBm but the LNA amplifies 36 dB, therefore 6 dBm is the RF signal from the leakage. In general, a mixer is saturated if the RF port power exceeds 10 dB less than the work point power at the LO. The IQ mixer works with 10 dBm LO, so 6 dBm RF is too high, so the usage of attenuators is reasonable.

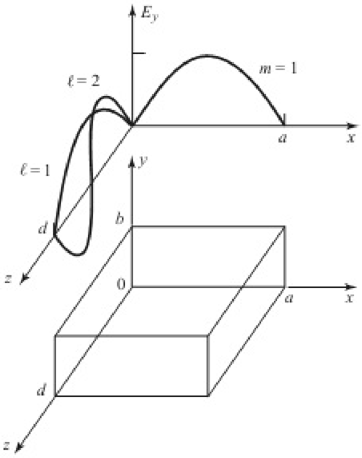

Figure B.1: A rectangular cavity resonator, and the electric field variations for the TE_{101} (l=1) and TE_{102} (l=2) resonant modes from Ref. [22]

Figure B.2: The entrance of the cavity with the flange and the coupler.

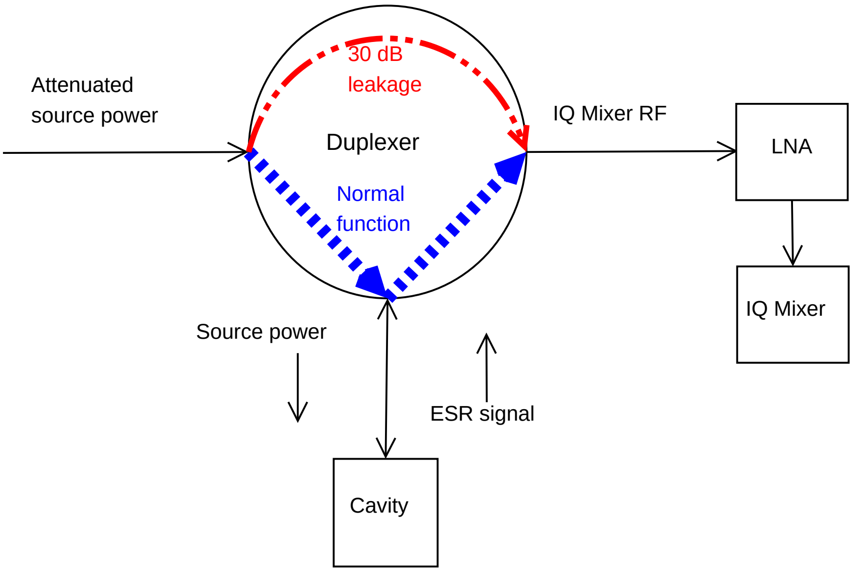

Figure B.3: Schematics of duplexer and its surroundings

Appendix C

Advantage of Low Noise Amplifiers

Attaining the best signal to noise ratio (SNR) is the priority in any branches of measurement science. Now we give a short explanation about general low noise measurement and the benefit of the use of LNAs according to Ref. [24, 25].

In 1942, Harald T. Friis, working in Bell Labs, developed the theory of "noise figure" (NF) to calculate the signal to noise ratio at the output of a complex receiver chain. Definition of NF of a device is

$$NF = 10\log_{10}\left(\frac{\mathrm{SNR_{in}}}{\mathrm{SNR_{out}}}\right) = 10\log_{10}(F) \tag{C.1}$$

where $\mathrm{SNR_{out}}$ and $\mathrm{SNR_{in}}$ are the output and input signal to noise power ratios, respectively. Noise figure is often used in microwave engineering but the noise factor is used for noise calculation. The noise factor is $F = \frac{\mathrm{SNR_{in}}}{\mathrm{SNR_{out}}}$. The SNR is the most convenient way of quantifying how much thermal noise the receiver adds to the signal. F is a measure of how the SNR is reduced by a device. The noise factor is correlated with the thermal noise power $P_{\mathrm{Thermal}} = k_{\mathrm{B}}T\Delta f$ which is -174 dBm at room temperature with 1 Hz bandwidth (where k_B) is the Boltzmann constant). Noise factor expresses how many times more noise we obtain at the output of a device. Depending on where devices are positioned in a complex receiver chain, the individual noise factors will have different effects on the overall noise, according to Friis's equation which gives the resultant noise factor of the receiver chain as:

$$F = F_1 + \frac{F_2 - 1}{G_1} + \frac{F_3 - 1}{G_1 G_2} + \frac{F_4 - 1}{G_1 G_2 G_3} + \cdots + \frac{F_n - 1}{G_1 G_2 G_3 \cdots G_{n-1}} \tag{C.2}$$

where G_i and F_i are the available power gain and noise factor, respectively, of the i-th stage, and n is the number of stages. The first amplifier in the chain has the most significant effect on the total noise figure than any other amplifier in the chain. The lowest noise figure amplifier has to go first in a line of amplifiers in order to get the lowest noise factor and the highest SNR. As an example, we calculate the noise figure of our quadrature detection system. We show the amplifier chain, mixer detector, and lock-in amplifier in Fig.C.1.

We need linear data for the resultant noise factor calculation: $F_i = 10^{\frac{NF_i[dB]}{10}}$, $G_i = 10^{\frac{G_i[dB]}{10}}$.

$$F = 1.412 + \frac{2.551 - 1}{39.812} + \frac{5.623 - 1}{39.812 \cdot 100} + \frac{63.096 - 1}{39.812 \cdot 100 \cdot 0.178} = 1.540 \quad \text{(C.3)}$$

and the resultant noise figure $NF = 10\log(1.54) = 1.9$ dB. We measured $15\frac{\mathrm{nV}}{\sqrt{Hz}}$ noise with lock-in amplifier during TESR experiments. The noise of the lock-in amplifier is $8\frac{\mathrm{nV}}{\sqrt{Hz}}$ at 100 kHz this gives NF=$10\log((15/8)^2)$=5.5 dB, but we measured at 20 kHz and the noise has 1/f scale, so we obtained a quantitatively right result.

The background of low noise LNA is the so-called high-electron-mobility transistor (HEMT) which was invented by Takashi Mimura in 1979 [26]. In HEMTs high mobility electrons are generated using the heterojunction of a highly doped wide-bandgap n-type donor-supply layer (often AlGaAs) and a non-doped narrow-bandgap channel layer with no dopant impurities (such as GaAs). HEMTs are able to operate at higher frequency and they brought revolutionary development in many applications where low noise and high gain at high frequencies are required (radio astronomy, radar etc.)[27, 28]. We note that in 1960's there were preamplifiers and Friis's equation was known but the devices operate with high noise level.

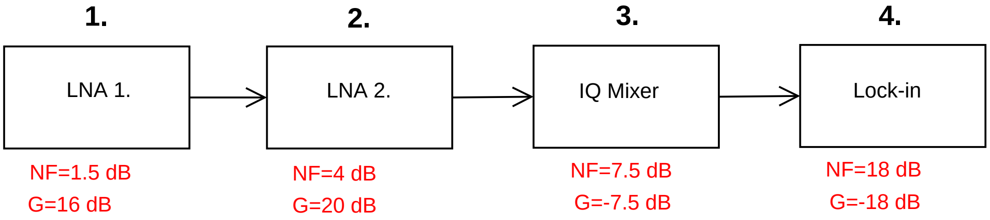

Figure C.1: Schematics of receiver chain.

Appendix D

Simulation of spin diffusion

We performed a simple quasi-classic simulation of spin diffusion. We placed the excited particles randomly in the skin depth. We assume that in the skin depth the excitation is homogeneous in space and time, because we only focus on the spin diffusion not ESR line shape.

In every step (which corresponds a unit τ) the particle moved one mean free-path unit in random direction in 3 dimensions. According to Dyson's assumptions an electron loses its spin state exponentially with respect to the time. Thus the number of excited spins decay with $e^{\frac{t}{T_1}}$, where t is the lasted time from the excitation. Hence in every step a random number was casted for every particle. If this number is less than $\frac{\tau}{T_1}$ the electron loses its excited state and it will not take part in the further simulation. We chose $T_1 = 10^5\tau$,$v_F = 1$, $\tau = 1$ and the mean free path is unit. In this scale the skin depth is $\delta_{\text{Skin}} = 90.9$. Therefore the normal skin effect is realized since the mean free path is smaller than δ_{Skin}. We run the simulation for 24000 particles with 150000 steps which corresponds $1.5T_1$ time. We assume that there is elastic collision with the walls and it has no effect on spin lifetime. The initial and final state of the simulation is shown in Fig. D.1.

Fig. D.2 shows that we fitted the distribution curve with $Ae^{\frac{x}{x_{\text{Decay}}}} + y_0$. We expect that x_{Decay} is close to the spin diffusion length which is $\frac{1}{\sqrt{3}}v_F\sqrt{\tau T_1} = 182$ mean free-path unit. From the fit we read $x_{\text{Decay}} = 203 \pm 16$. This simple model gives a qualitatively correct result which corresponds to Dyson's assumptions. We note that this simple approach is only valid when the spin- orbit coupling is weak enough.

The simulation is written in Python and is given below along with some simulation results.

```python
# coding=utf-8
from random import randint
import timeit
import math

FREE_PATH = 1
number_of_electrons =24000
electrons = []





class box:
    def __init__(self,origo = [],diagonal_point = []):
        self.origo = origo
        self.diagonal_point = diagonal_point
    def return_random(self):  # choose random point in the box between origo and diagonal_point
        return [uniform(self.origo[0],self.diagonal_point[0]),
                uniform(self.origo[1],self.diagonal_point[1]),
                uniform(self.origo[2],self.diagonal_point[2])]


class e_part:
    def __init__(self, spin, coordinate = []):
        self.coordinate = coordinate
        self.spin = spin
    def move_step(self,inbox = box([0, 0, 0],[10, 10, 10])):
        dz_coord = uniform(-FREE_PATH,FREE_PATH)
        phi = uniform(0,1)
        dx_coord = math.sqrt((FREE_PATH*FREE_PATH)-dz_coord*dz_coord)* math.cos(2*math.pi*phi)
        dy_coord = math.sqrt((FREE_PATH*FREE_PATH)-dz_coord*dz_coord)* math.sin(2*math.pi*phi)
        self.coordinate[0] = self.coordinate[0] + dx_coord
        self.coordinate[1] = self.coordinate[1] + dy_coord
        self.coordinate[2] = self.coordinate[2] + dz_coord
        #print("collisions with walls")
        #X collisions
        if(self.coordinate[0] < inbox.origo[0]):
            self.coordinate[0] = 2*inbox.origo[0] - self.coordinate[0]
        if(self.coordinate[0] > inbox.diagonal_point[0]):
            self.coordinate[0] = 2*inbox.diagonal_point[0] - self.coordinate[0]
        #Y collisions
        if(self.coordinate[1] < inbox.origo[1]):
          self.coordinate[1] = 2*inbox.origo[1] - self.coordinate[1]

        if(self.coordinate[1] > inbox.diagonal_point[1]):
            self.coordinate[1] = 2*inbox.diagonal_point[1] - self.coordinate[1]

        #Z collisions
        if(self.coordinate[2] < inbox.origo[2]):
            self.coordinate[2] = 2*inbox.origo[2] - self.coordinate[2]

        if(self.coordinate[2] > inbox.diagonal_point[2]):
```

```
            self.coordinate[2] = 2*inbox.diagonal_point[2] - self.coordinate[2]


    def check_in_box (self,inbox = box([0,0,0],[10,10,10])):
        return ((inbox.origo[0]< self.coordinate[0]< inbox.diagonal_point[0] )and (inbox.origo[1
        ]< self.coordinate[1]< inbox.diagonal_point[1])and (inbox.origo[2]< self.coordinate[2]<
        inbox.diagonal_point[2]))


def main():
    f = open('sim.txt','w')
    start = timeit.default_timer()
    sum = 0
    start_box = box([0,0,0],[90.9,909090,909090])
    end_box = box([2636,0,0],[2727,909090,909090])
    full_box = box([0,0,0],[2727,909090,909090])
    electrons = []   #create a list
    for count in range(1,number_of_electrons):
        electron_item = e_part(1,start_box.return_random())
        electron_item.attr = count
        electrons.append(electron_item)
    for t in range(1,150000):  ##about 1.5*T1 time
        for electron in electrons:
            if (uniform(0,1000000)<10 ):

                electrons.remove(electron)

            electron.move_step(full_box)

    for electron in electrons:
        print electron.coordinate[0] #

        if(electron.check_in_box(full_box)):
                f.write(str(t)) #write t and coordinates when an electron lives
                f.write('\t')
                f.write(str(electron.coordinate[0]))
                f.write('\t')
                f.write(str(electron.coordinate[1]))
                f.write('\t')
                f.write(str(electron.coordinate[2]))
                f.write('\n')
                sum += 1
    print sum
    f.close()
    stop = timeit.default_timer()
    print "runtime:" + str(stop - start )


if __name__ == "__main__": main()
```

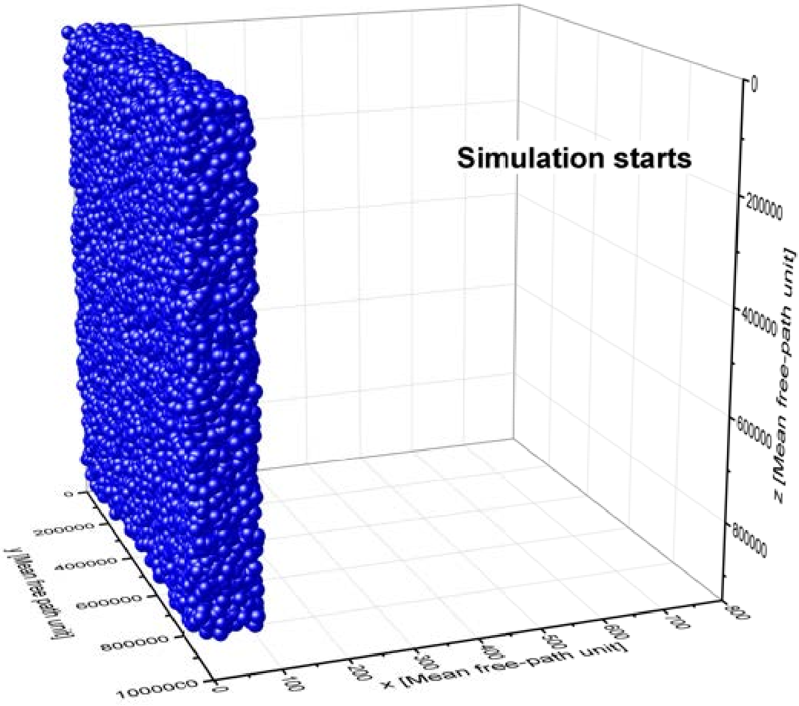

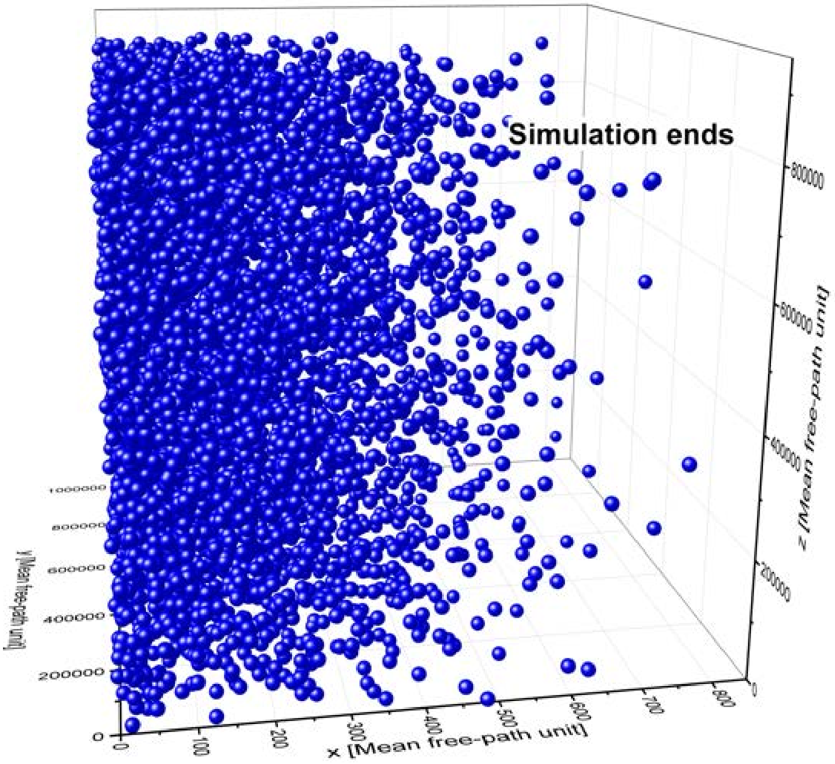

Figure D.1: Spatial distribution of electrons before and after the simulation

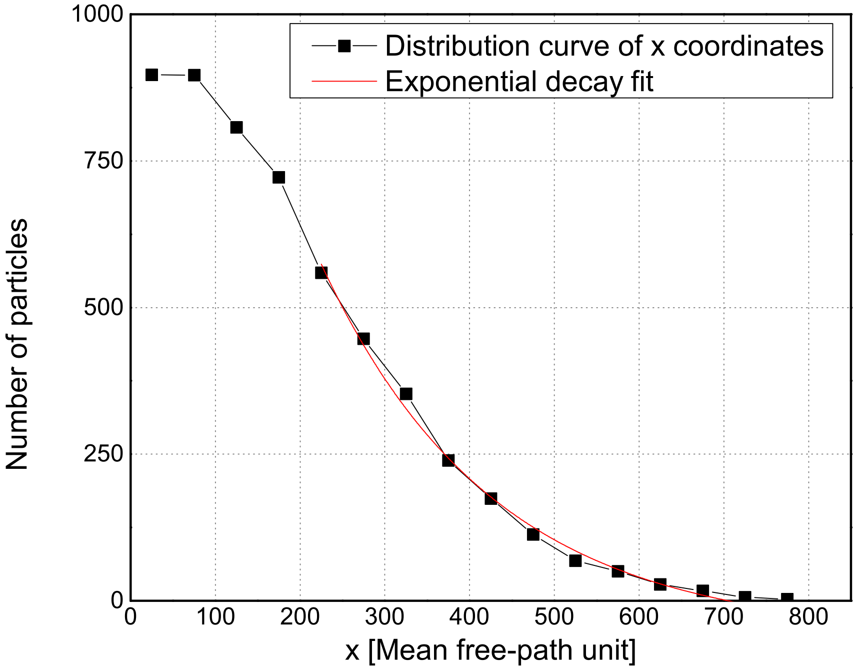

Figure D.2: Distribution curve and fitted line from the histogram of x coordinates.

Bibliography

[1] Y. K. Zavoisky, Paramagnetic Absorption in Perpendicular and Parallel Fields for Salts, Solutions and Metals, PhD thesis, Kazan State University, 1944

[2] F. Bloch, “Nuclear induction",Phys. Rev., vol. 70, pp. 460–474, Oct 1946.

[3] I. Žutić, J. Fabian, and S. D. Sarma, “Spintronics: Fundamentals and applications,” Rev. Mod. Phys., vol. 76, pp. 323–410, 2004.

[4] F. J. Dyson, “Electron Spin Resonance Absorption in Metals. II. Theory of Electron Diffusion and the Skin Effect,”Physical Review, vol. 98, p. 349, 1955.

[5] G. Feher and A. F. Kip, “Electron Spin Resonance Absorption in Metals. I. Experimental,” Physical Review, vol. 98, p. 337, 1955.

[6] M. Ya.Azbel’, V.I. Gerasimenko, and I. M.Lifshitz, Zh. Eksperim. i. Teor. Fiz.32, 1212(1957) [translation: Soviet Phys. —JETP5, 986(1957)

[7] R.B. Lewis and T.R. Carver, Conduction electron spin resonance in lithium Phys. Rev. Letters 12, 693(1964)

[8] T. H. Wilmshurst: Electron Spin Resonance Spectrometers (Monographs on electron spin resonance) London : Hilger, 1967.

[9] http://www.ittc.ku.edu/ jstiles/622/handouts/Mixer%20Conversion%20Loss.pdf 2015.05.15.

[10] http://www.markimicrowave.com/blog/2013/06/iq-image-reject-and-single-sideband-mixers/ 2015.05.16.

[11] N. S. VanderVen and R.T. Schumacher, Resonant transmission of microwave power through "thick" films of lithium metal Phys. Rev. Letters 12, 695(1964)

[12] Jerome I. Kaplan, Application of the Diffusion-Modified Bloch Equation to Electron Spin Resonance in Ordinary and Ferromagnetic Metals, Phys. Rev. 115, 575 (1959)

[13] R. de L. Kronig, "On the theory of the dispersion of X-rays". J. Opt. Soc. Am. 12: 547–557 (1926)

[14] H.A. Kramers, "La diffusion de la lumiere par les atomes". Atti Cong. Intern. Fisici (1927)

[15] Hilbert David Grundzüge einer allgemeinen Theorie der linearen Integralgleichungen, Chelsea Pub. Co. (1953)

[16] B.V. Khvedelidze, "Hilbert transform", in Hazewinkel, Michiel, Encyclopedia of Mathematics, Springer (2001)

[17] András Jánossy, Resonant and nonresonant conduction-electron-spin transmission in normal metals, Phys.Rev. B 21,3793 (1970)

[18] Pandey, J.N. (1996), The Hilbert transform of Schwartz distributions and applications, Wiley-Interscience

[19] R. J. Pressley and H. L. Berk, g Factor of Conduction Electrons in Metallic Lithium, Phys. Rev. 140. A1207,(1965)

[20] Charles P. Poole, Electron Spin Resonance – A Comprehensive Treatise on Experimental Techniques, Interscience Publishers 1967

[21] John D. Kraus, Electromagnetics, McGraw-Hill Companies 1992,

[22] David Pozar, Microwave Engineering, John Wiley & Sons, Inc.

[23] http://en.wikipedia.org/wiki/Impedance_matching 2015.05.20.

[24] J.D. Kraus, Radio Astronomy, McGraw-Hill, 1966

[25] http://www.microwaves101.com/encyclopedias/noise-figure 2015.05.20.

[26] Takashi Mimura: 'The Early History of the High Electron Mobility Transistor (HEMT)',IEEE TRANSACTIONS ON MICROWAVE THEORY AND TECHNIQUES, VOL. 50, NO. 3, MARCH 2002

[27] http://www.semiconductor-today.com/news_items/2014/OCT/NORTHROP-GRUMMAN_311014.shtml 2015.05.18.

[28] http://en.wikipedia.org/wiki/High-electron-mobility_transistor#cite_note-2 2015.05.15.

[29] N. Tombros, C. Józsa, M. Popinciuc, H. T. Jonkman, and B. J. van Wees, Nature (London) 448, 571 (2007).

[30] N. Tombros, S. Tanabe, A. Veligura, C. Jozsa, M. Popinciuc, H. T. Jonkman, and B. J. van Wees Phys. Rev. Lett. 101, 046601